Memoirs of the Faculty of Engineering, Nagoya University
Vol. 37, No. 2 (1985)

ON THE VORTEX BREAKDOWN PHENOMENA IN A SWIRLING PIPE-FLOW

TADAYA ITO, YOSHIKAZU SUEMATSU
and TOSHIYUKI HAYASE

Department of Mechanical Engineering II

(Received October 31, 1985)

Abstract

An abrupt change of flow pattern is possible to occur at a certain position along the axis in a swirling flow field, when the azimuthal velocity is relatively large as compared with the axial velocity. The phenomena are known as the vortex breakdown. The aim of the present research is to clarify the essential properties of the phenomena, and to obtain reasonable explanation to the multiformity of the breakdown form as well. First, the elastoid-inertia oscillation of the rotating fluid in a cylindrical vessel is examined experimentally and theoretically. As the result, some characters of the inertial wave in rotating fluid are clarified. Then the vortex breakdown phenomena in a circular pipe are investigated. In consequence, it is found that breakdown of various types correspond to the values of a parameter s which defines the azimuthal mode of the inertial wave disturbance. And it is also made clear that the breakdown of stationary type and unsteady one, observed to date, have close relation to the occurrence of inertial wave disturbances with and without phase velocity, respectively. The propriety of these conceptions is confirmed by experiments.

CONTENTS

1. Experiments on the Elastoid-Inertia Oscillations of a Rigidly Rotating Fluid in a Cylindrical Vessel

1. 1. Introduction

From a viewpoint of mechanical engineering the study of swirling flow field is very important in relation to various hydraulic machines, so investigations have been made on many aspects of swirling flows. One of the characteristic phenomena in swirling flows is the occurrence of internal waves or inertial waves. A number of hydraulic problems have been explained on the basis of inertial wave theory: for example, Kito[1] treated vibrations in draft tube of water turbine, Suzuki[2] reported on the sound of a peculiar frequency in vortex tube. And in authors' conception, the knowledge of inertial waves is very important and useful to clarify the vortex breakdown phenomenon which is the subject of this research. So we treat at first the elastoid-inertia oscillation, which is fundamental phenomenon relating to the inertial waves.

The possibility of occurrence of inertial wave in swirling flows was first pointed out by Lord Kelvin.[3] Later this inertial wave was reported to be of meteorological interest in relation to the problems of a rotating flow field (e. g., large-scale atmospheric and oceanic flow affected by the revolution of the earth). Theoretical studies of the inertial waves were made by the Bjerkness,[4] Solberg, and more recently by Greenspan.[5] Lord Rayleigh, Taylor and Chandrasekar investigated flow instabilities in terms of the growth or decay of inertial (or internal) waves.

On the other hand, some experimental verifications of the theoretical results have been made. Long[6] studied the inertial waves induced in the wake of a sphere moving along the axis in a rotating cylinder. Görtler and Oser[7] excited the inertial waves by means of an oscillating disk in a rotating cylinder, and visualized them by small flat aluminium particles in a fluid. In relation to the thermal convection, Fultz[8] investigated a standing-wave oscillation of inertial wave, which is called elastoid-inertia oscillation, in a rotating cylinder. And he realized its axisymmetrical mode by means of a forced oscillation with small circular disk. Fultz also ascertained that the natural frequencies of the axisymmetrical oscillation agreed well with the theoretically expected value.

It is known that the inertial wave in a rotating cylinder has several modes in the radial, azimuthal and axial directions. However, the flow patterns of the inertial waves of different modes have not been reported in detail to date. It is important to examine the characteristic patterns of the swirling flows due to inertial waves. And the validity of the theory should also be examined by experiments with respect to flow patterns. In this chapter, we deal with the elastoid-inertia oscillations in a rotating cylinder, which is one of the fundamental phenomena occurring with inertial waves. The flow patterns and natural frequencies of

the oscillations for several modes are examined by means of flow visualization. The experimental results are compared with those of inviscid-linear theory, a certain part of which are presented here for the first time.

1. 2. Inviscid Linear Theory of Elastoid-inertia Oscillation

As mentioned above, there are some reports which have dealt with the elastoid-inertia oscillations theoretically. In these reports the expression of the oscillatory flow field and natural frequencies have been presented on the assumption that the fluid is incompressible and inviscid. The former reports, however, only proposed the expressions, so the patterns and other properties of the flow field were not elucidated. The recent study by Fultz[8] is still confined to the simplest axisymmetric mode of oscillations, presenting its streamline patterns.

The expressions for the elastoid-inertia oscillations in a cylindrical vessel are herewith introduced as a prologue to later argument. The flow patterns and other properties of the oscillation including higher modes are described in more detail than in any previous report.

1. 2. 1. Expressions of Oscillations

The present analysis adopts a stationary cylindrical coordinate system (Fig. 1. 1), instead of a rotatory coordinate system used in former studies. The stationary coordinate system has an advantage in the comparison of flow patterns obtained from experiment and analytical results.

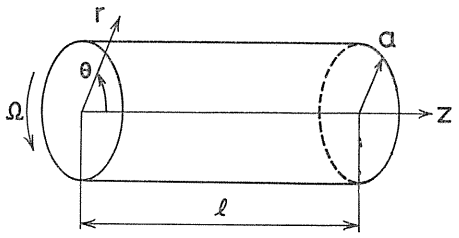

Fig. 1. 1 Cylindrical coordinate system.

The following are assumed in the analysis: (1) The fluid is incompressible and inviscid. (2) The primary steady flow, which does not contain the inertial waves, is a solid-body rotation without an axial velocity component. (3) The velocity fluctuations due to the inertial waves are small as compared with the azimuthal velocity of the primary flow.

The velocity components are denoted by u, v, w in the directions r, θ, z of the cylindrical coordinates and the pressure by p. These are expressed as the sum of the primary flow and the fluctuation as follows.

$$\left.\begin{aligned} &u=\tilde{u}(r,\ \theta,\ z,\ t),\ v=\Omega r+\tilde{v}(r,\ \theta,\ z,\ t)\\ &w=\tilde{w}(r,\ \theta,\ z,\ t)\\ &p=p_0+(1/2)\rho\Omega^2r^2+\tilde{p}(r,\ \theta,\ z,\ t)\end{aligned}\right\} \qquad (1.1)$$

where Ω is angular velocity of primary rotating flow, p_0 pressure at the axis of the cylinder, ρ density of fluid, t time, and the superscript tild indicates the fluctuation component.

Governing equations for an incompressible, inviscid fluid flow are Euler's equations of motion and an equation of continuity [see assumption (1)]. Substituting Eq. (1. 1) into these governing equations and referring to the assumption (3), we obtain a set of four linearized equations with respect to the fluctuations $\tilde{u}$, $\tilde{v}$,

$\tilde{w}$ and $\tilde{p}$. The fluctuations are put in the following complex form:

$$\left.\begin{aligned}\tilde{u}(r,\ \theta,\ z,\ t) &= U(r)\, e^{i(nt-s\theta-mz)}\\ \tilde{v}(r,\ \theta,\ z,\ t) &= V(r)\, e^{i(nt-s\theta-mz)}\\ \tilde{w}(r,\ \theta,\ z,\ t) &= W(r)\, e^{i(nt-s\theta-mz)}\\ \tilde{p}(r,\ \theta,\ z,\ t) &= P(r)\, e^{i(nt-s\theta-mz)}\end{aligned}\right\} \tag{1.2}$$

where m is wave number in the axial direction (real number), s wave number in the azimuthal direction (0 or positive integer), i imaginary unit, n circular frequency (real number), U(r), V(r), W(r), and P(r) are complex functions of r. Substituting Eq. (1.2) into the linearized equations for fluctuations, we obtain a system of ordinary differential equations for U, V, W and P. These are integrated analytically and the complex solutions of the fluctuations are determined. Taking the real part, we obtain the real solutions as follows:

$$\left.\begin{aligned}\tilde{u} &= A(m/\sigma)\left[J_{s-1}(\sigma r) - \left\{\frac{2\Omega+(n-s\Omega)}{n-s\Omega}\right\}\right.\\ &\quad\left.\times\left(\frac{s}{\sigma r}\right)J_s(\sigma r)\right]\sin(nt-s\theta-mz)\\ \tilde{v} &= A\frac{m/\sigma}{n-s\Omega}\left[2\Omega J_{s-1}(\sigma r) - \left(\frac{s}{\sigma r}\right)\right.\\ &\quad\left.\times\{2\Omega+(n-s\Omega)\}J_s(\sigma r)\right]\cos(nt-s\theta-mz)\\ \tilde{w} &= AJ_s(\sigma r)\cos(nt-s\theta-mz)\\ \tilde{p}/\rho &= A\frac{n-s\Omega}{m}J_s(\sigma r)\cos(nt-s\theta-mz)\end{aligned}\right\} \tag{1.3}$$

where A is fluctuation amplitude (arbitrary real number), J_s is the sth-order Bessel function of the first kind and σ is defined as

$$\sigma^2 = m^2\{4\Omega^2-(n-s\Omega)^2\}/(n-s\Omega)^2 \tag{1.4}$$

From the boundary condition ($\tilde{u}=0$ at $r=a$, a: radius of the cylinder), the eigenvalue σ is determined as the root of the following characteristic equation:

$$J_{s-1}(\sigma a)/J_s(\sigma a) = (s/\sigma a)\{1\pm\sqrt{1+(\sigma/m)^2}\} \tag{1.5}$$

For either sign on the right side, the above equation has an infinite number of positive eigenvalues denoted by $\sigma_{\pm g}$ ($g=1,\ 2,\ 3\ \cdots$) in the order of magnitude, where the double sign at g corresponds to the sign in Eq. (1.5).

Displacing the axial wave number m by $-m$ in Eq. (1.3), we obtain another solution with the same values of n and σ [see Eqs. (1.4) and (1.5)]. These represent a pair of forward and backward progressive waves with the same wave length. As the sum of these solutions for each fluctuation component, an ex-

pression of the elastoid-inertia oscillation is obtained as follows:

$$\left.\begin{aligned}
\tilde{u} &= c\,(m/\sigma)\left[J_{s-1}(\sigma r) - \frac{\{2\Omega+(n-s\Omega)\}}{(n-s\Omega)}\left(\frac{s}{\sigma r}\right)\right. \\
&\quad \left.\times J_s(\sigma r)\right]\sin(nt-s\theta)\cos mz \\
\tilde{v} &= c\frac{m}{(n-s\Omega)\sigma}\left[2\Omega J_{s-1}(\sigma r) - \left(\frac{s}{\sigma r}\right)\right. \\
&\quad \left.\times\{2\Omega+(n-s\Omega)\}J_s(\sigma r)\right]\cos(nt-s\theta)\cos mz \\
\tilde{w} &= cJ_s(\sigma r)\sin(nt-s\theta)\sin mz \\
\tilde{p}/\rho &= c\frac{(n-s\Omega)}{m}J_s(\sigma r)\cos(nt-s\theta)\cos mz
\end{aligned}\right\} \qquad (1.6)$$

where $C=2A$. From the boundary condition at both ends of the cylinder with rigid walls ($\tilde{w}=0$ at $z=0$ and l, l: length of cylindrical vessel), the value of m is determined as

$$m=(k\pi/l), \quad (k=1,\ 2,\ 3,\ \cdots)$$

Circular frequency $n_{\pm g}$, which corresponds to $\sigma_{\pm g}$, is described from Eq. (1.4) as follows:

$$n_{\pm g}=s\Omega\pm 2\Omega\sqrt{m^2/(m^2+\sigma_{\pm g}^2)} \qquad (1.7)$$

The double sign at the second term on the right-hand side of the expression, corresponding to the sign of $\pm g$, suggests the existence of two different series of values of n in general, though in the case of $s=0$ their absolute values coincide with each other and double sign only means 180° shift in phase. In the coordinate system rotating with the cylinder the properties of the oscillation are determined as follows. The azimuthal coordinate is transformed by

$$\theta-\Omega t=\theta'$$

where θ' is an azimuthal coordinate based on a rotatory frame. Referring to the relation such as

$$\sin(nt-s\theta)=\sin\{(n-s\Omega)t-s\theta'\} \qquad (1.8)$$

we obtain the circular frequency in a rotatory coordinate system:

$$n'_{\pm g}=n_{\pm g}-s\Omega=\pm 2\Omega\sqrt{m^2/(m^2+\sigma_{\pm g}^2)} \qquad (1.9)$$

This expression shows that the absolute value of the circular frequency in the rotatory system never exceeds 2Ω.

1. 2. 2. Flow Patterns of Oscillations

In this section the flow patterns and other properties of several oscillatory modes are theoretically examined in preparation for the experimental analysis. At first characteristics of the flow field will be described in general. The flow pattern of the elastoid-inertia oscillation is distinguished by three parameters, namely (s, g, k) [see Eq. (1. 6)]. The parameters s, g, k determine the flow mode in the azimuthal direction (θ-direction), in the radial direction (r-direction), and in the axial direction (z-direction), respectively.

In the axial direction the flow field is divided into cells by nodal planes normal to the z-axis. The nodal planes, on which the axial velocity component $\tilde{w}$ vanishes, are l/k apart from each other, so the number of planes is $(k-1)$ [see Eq. (1. 6)]. In the radial direction the flow field is divided into parts by cylindrical surfaces, where no radial velocity component $\tilde{u}$ exists. The nodal radii of the cylindrical surfaces are derived from the following equation.

$$J_{s-1}(\sigma_g r)/J_s(\sigma_g r)=[1+2\Omega/(n-s\Omega)](s/\sigma_g r) \tag{1.10}$$

and the number of the surfaces is $(g-1)$ [see Eq. (1. 6)].

In the azimuthal direction a geometrical symmetry of the flow field appears around the axis of the cylinder. Owing to Eqs. (1. 6) and (1. 8), a velocity vector $\vec{V}$ on the rotatory coordinate system satisfies the relation as

$$\vec{V}[t,\ r,\ \theta',\ z]=\vec{V}[t,\ r,\ \theta'+(2\pi/s),\ z] \tag{1.11}$$

Therefore the flow field has a rotational symmetry with a rotation of $(360/s)$ degrees on the axis. In particular for the fundamental mode of $s=0$ the velocity vector is independent of the azimuthal coordinate θ, and so the flow field is axisymmetrical. These results, of course, are still valid in the stationary coordinate system.

For $s\neq 0$ mode the velocity field, whose symmetrical structure is examined above, rotates steadily on the z-axis. The angular velocity of rotation is n/s in the stationary system or $n'/s=(n-s\Omega)/s$ in the rotatory system [see Eq. (1. 8)]. For $s=0$ mode the axisymmetrical velocity field fluctuates with a circular frequency n in both the stationary system and the rotatory one.

Streamlines and pathlines are calculated as follows. The equation of the streamline in the stationary system is expressed as

$$dr/u=rd\theta/v=dz/w \tag{1.12}$$

Referring to Eqs. (1. 1) and (1. 6), we obtain the streamline configuration through a numerical integration of the above equation. Displacing the azimuthal coordinate θ by θ' in the expressions, we can also obtain the streamlines in the rotatory coordinate system.

Neglecting the azimuthal or axial velocity component in Eq. (1. 12), we obtain a sectioned-streamline as the section of a stream surface (envelope of streamlines) by a plane through the axis (r-z plane) or normal to the axis (r-θ plane). In the stationary coordinate system the pattern of sectioned-streamlines on the r-θ plane coincides with the original pattern by a rotation of $(360/s)°$ on the z-axis similar to the velocity field. On the other hand the sectioned-streamlines in the rotatory system coincide with the original one by a rotation of $(180/s)°$, or the half of the

above rotation [see Eqs. (1.1), (1.6), (1.8) and (1.12)].

A pathline in the stationary system is obtained through a numerical integration of the equation

$$\left.\begin{aligned} dr/dt&=u\\ rd\theta/dt&=v\\ dz/dt&=w \end{aligned}\right\} \tag{1.13}$$

where θ should be displaced by θ' for the case of the rotatory system.

In the discussion given below all the quantities are expressed in dimensionless form as follows:

$$\left.\begin{aligned} &R=r/a,\ Z=z/a,\ L=l/a,\ U=u/a\Omega\\ &V=v/a\Omega,\ W=w/a\Omega,\ M=am,\ T=\Omega t\\ &N=n/\Omega,\ N'=n'/\Omega,\ \overline{\Omega}=\Omega/\Omega,\ C=c/a\Omega \end{aligned}\right\} \tag{1.14}$$

In the stationary system the circular frequency N is determined from Eq. (1.7) for the dimensionless cylinder length L, which corresponds to the half of a wave length for a fundamental axial mode [$k=1$, see Eq, (1.6)]. The natural circular frequencies N are given in Fig. 1.2 by solid lines for the azimuthal mode $s=0$, 1, 2, respectively, with axial and radial fundamental modes, and by chain lines for the case of $s=0$ with its axial and radial higher modes. Plots of circular symbols are experimental data which will be mentioned later.

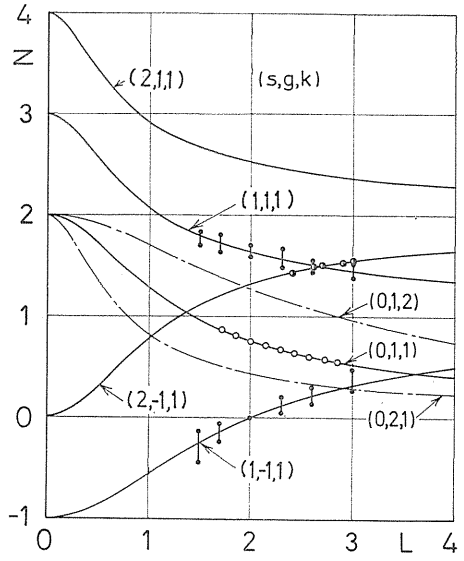

Fig. 1.2. Natural circular frequency versus length of cylindrical vessel.

As stated above, the characteristic of the flow field is greatly affected by the azimuthal flow mode, or by the value of s. Thus, the flow field is examined below for $s=0$, 1 and 2, separately. Except for the $s=0$ mode the discussion is here confined to the fundamental modes in the radial and axial directions ($g\pm1$, $k=1$).

1. 2. 2. 1. Streamlines of Axisymmetric Mode ($s=0$ Mode)

For the mode of (s, g, k)=(0, 2, 1), axisymmetric sectioned-streamlines by the R-Z plane have already been calculated by Fultz. Here the flow patterns of $s=0$ mode, including the similar one by Fultz,[8] are treated.

Figure 1.3 shows the sectioned-streamlines by the plane through the Z-axis for (s, g, k)=(0, 2, 1). The pattern itself does not change with the passage of time. The flow field is separated into cells by a nodal cylindrical surface (indi-

cated by broken lines) through which no fluid particle passes. The flow pattern is omitted outside of the nodal surface in the left half of the figure. If the cylindrical wall is just on the nodal surface, the flow inside is transformed into the fundamental mode, namely $(s, g, k) = (0, 1, 1)$. Arrows along the streamlines indicate the direction of movement at the same instant. The velocity vector changes its magnitude and sense periodically, though the incline of the vector (corresponding to the tangent of the streamline) does not change with time.

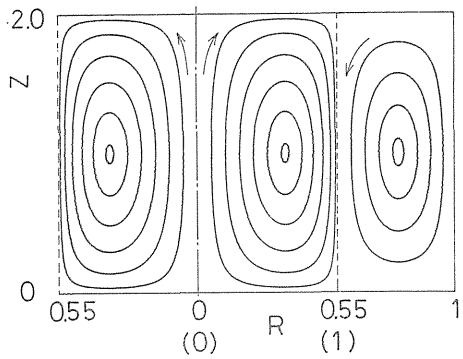

$L=2$, $M=1.571$, $N=0.7586$, $C=1.0$

Fig. 1.3. Sectioned-streamlines on the R-Z plane for axisymmetric oscillation.

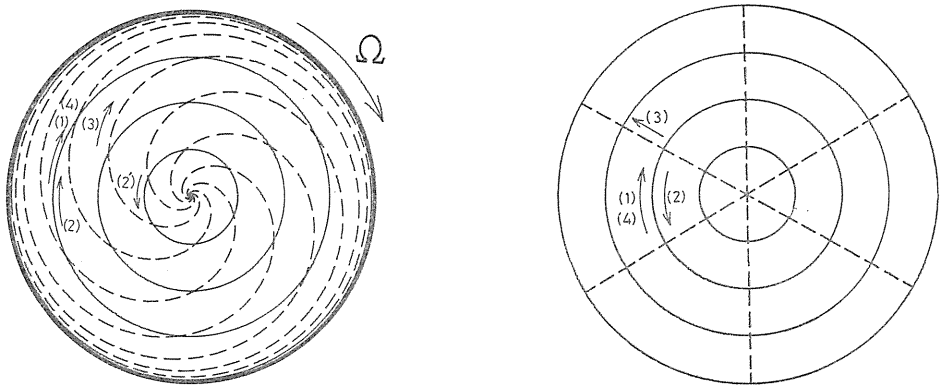

(a) In stationary system. (b) In rotatory system.

$L=2.0$, $M=1.571$, $N=0.7586$, $C=1.0$

Fig. 1.4. Sectioned-streamlines on the R-θ plane for $s=0$ mode oscillation.

Figure 1.4 shows the sectioned-streamlines by the plane normal to the Z-axis located at the end of the cylinder, where the axial velocity component vanishes, and so the sectioned-streamline is identical with the streamline. Streamlines for (0, 1, 1) mode at several instants in a period are calculatd in the stationary system [Fig. 1.4 (a)] and in the rotatory system [Fig. 1.4 (b)]. In Figs. 1.4 (a) and (b), solid lines are the streamlines for the phase $NT(=nt)$ of 0, and broken lines for the phase of $3\pi/2$. Numbered arrows (1)~(4) show the directions of fluid motion at the phases $NT=0$, π, $(3/2)\pi$ and 2π, respectively. The pattern of the sectioned-streamlines at a different axial position is also similar to the pattern described above.

1. 2. 2. 2. Streamlines of $s=1$ Mode

For $s\neq 0$ mode, as mentioned before, the velocity field rotates on the Z-axis with the angular velocity N/s in the stationary system or N'/s in the rotatory system. And there exist two different types of oscillation corresponding to the

radial modes $\pm g$. In this section streamlines of $s=1$ mode are calculated numerically for the fundamental modes $(g, k)=(1, 1)$ and $(-1, 1)$.

Sectioned-streamlines for the mode $(s, g, k)=(1, 1, 1)$ are described in Figs. 1. 5 (a) to (c). Figure 1. 5 (a) shows the streamlines on the plane through the

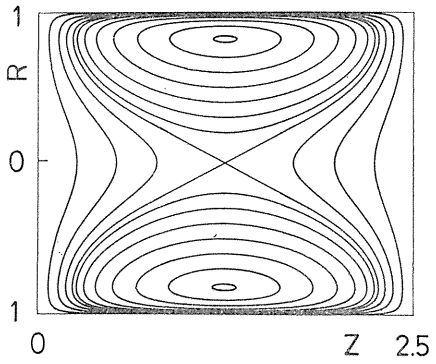

(a) On the R-Z plane.

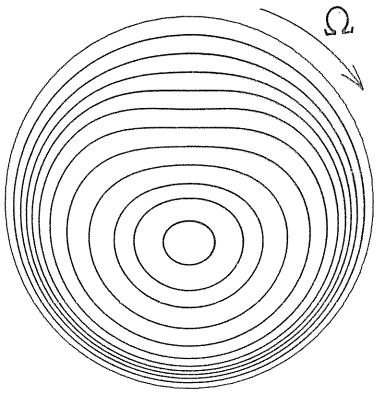

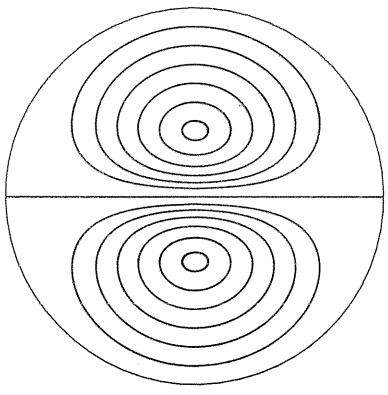

(b) In stationary system. (c) In rotatory system.

$L=2.5$, $M=1.257$, $N=1.521$, $N'=0.521$, $C=1.0$

Fig. 1. 5. Sectioned-streamlines for $(s, g, k)=(1, 1, 1)$ mode oscillation.

Z-axis. The flow pattern is independent of time T, azimuthal coordinate θ (or θ'), and also the adopted coordinate system (either the stationary system or the rotatory one). Sectioned streamlines by the plane normal to the Z-axis with the same condition as above are calculated both in the stationary system and the rotatory one, shown in Figs. 1. 5 (b) and (c). The plane is located at the cylinder end ($Z=2.5$) where no axial velocity component $\tilde{w}$ exists, so that the sectioned-streamlines are identical with the streamlines themselves. These patterns rotate steadily with the angular velocity N [Fig. 1. 5 (b)] or N' [Fig. 1. 5 (c)] on the Z-axis.

Figures 1. 6 (a) to (c), corresponding to Figs. 1. 5 (a) to (c), show the sectioned-streamlines of the other type for the mode $(s, g, k)=(1, -1, 1)$, it is noted that the sectioned-streamlines by the plane through the Z-axis in Fig. 1. 6 (a) greatly differ in their pattern from the ones in Fig. 1. 5 (a).

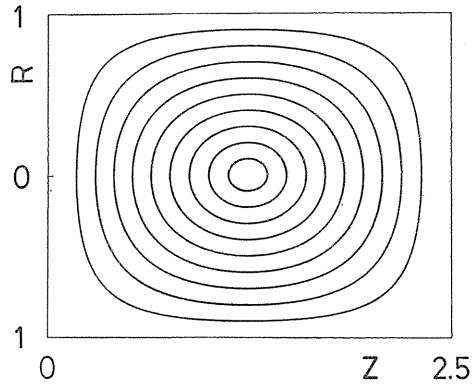

(a) On the R-Z plane.

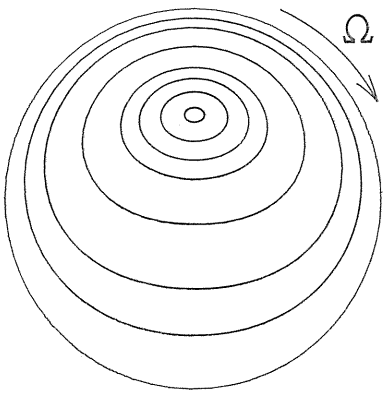

(b) In stationary system.

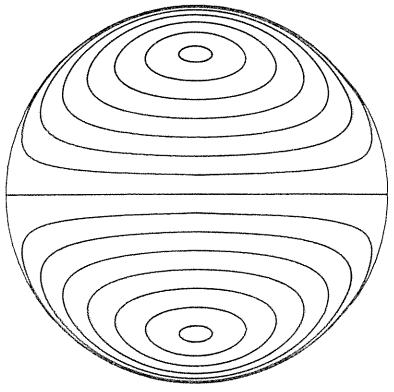

(c) In rotatory system.

$L=2.5$, $M=1.257$, $N=0.1925$, $N'=-0.8075$, $C=1.0$

Fig. 1. 6. Sectioned-streamlines for $(s, g, k)=(1, -1, 1)$ mode oscillation.

1. 2. 2. 3. Streamlines of $s=2$ Mode

Sectioned-streamlines of $s=2$ mode are shown for $(s, g, k)=(2, 1, 1)$ in Figs. 1.7 (a) to (c) and for $(2, -1, 1)$ in Figs. 1.8 (a) to (c), respectively. In the same manner to the case of $s=1$, the pattern of sectioned-streamlines on the plane through the Z-axis is independent of time T and inclination angle of the plane $\theta(\theta')$ [Figs. 1.7 (a) and 1.8 (a)]. And the streamlines on the plane normal to the axis rotate steadily with the angular velocity $N/2$ [Figs. 1.7 (b) and 1.8 (b), in the stationary system] or $N'/2$ [Figs. 1.7 (c) and 1.8 (c), in the rotatory system].

In spite of the theoretical assumption of small perturbation, the fluctuation amplitude in the above calculation is chosen as large as the primary flow to show clearly the characteristics of the oscillation.

1. 3. Experiment

The elastoid-inertia oscillation is herewith investigated experimentally, and the visualized flow fields of elastoid-inertia oscillation are compared with the results of the inviscid-linear theory.

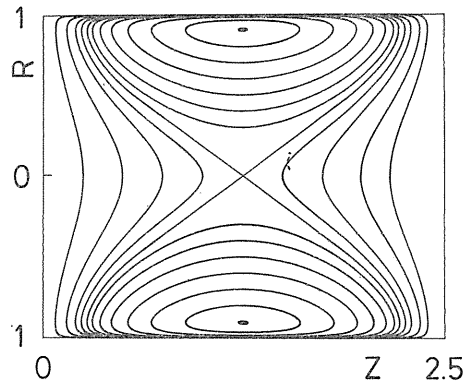

(a) On the R-Z plane.

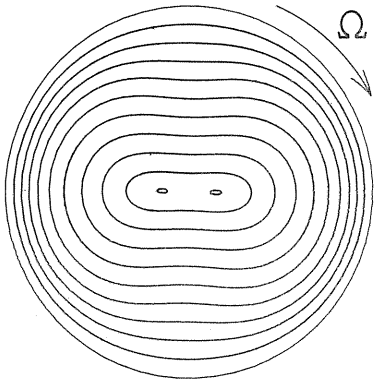

(b) In stationary system.

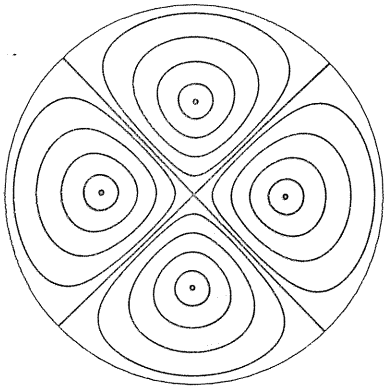

(c) In rotatory system.

$L=2.5$, $M=1.257$, $N=2.4329$, $N'=0.4329$, $C=1.0$

Fig. 1. 7. Sectioned-streamlines for $(s, g, k)=(2, 1, 1)$ mode oscillation.

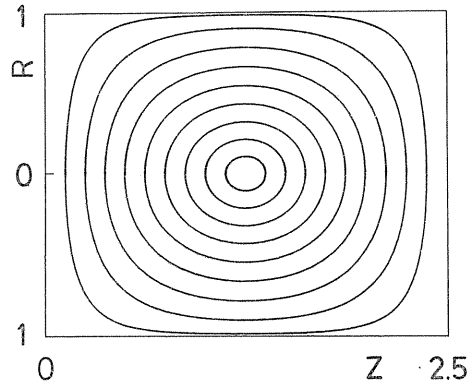

(a) On the R-Z plane.

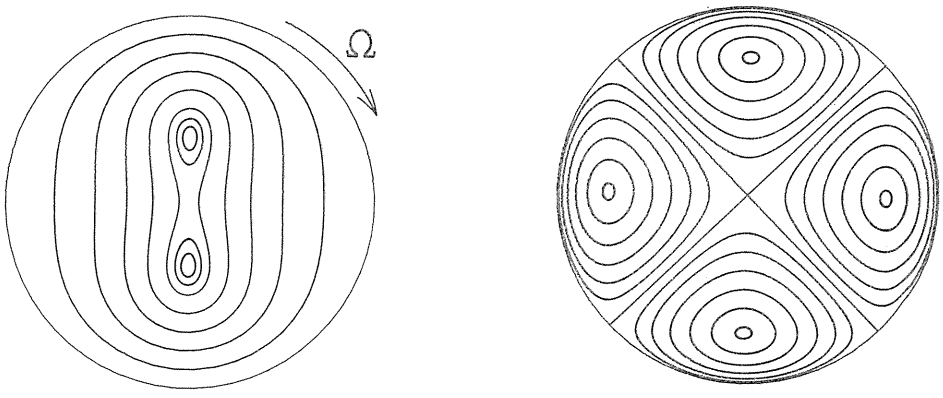

(b) In stationary system. (c) In rotatory system.

$L=2.5$, $M=1.257$, $N=1.4675$, $N'=-0.5325$, $C=1.0$

Fig. 1. 8. Sectioned-streamlines for $(s, g, k)=(2, -1, 1)$ mode oscillation.

1. 3. 1. Experimental Apparatus

A schematic view of the experimental apparatus is shown in Fig. 1. 9. A transparent acrylic cylinder C of inside diameter 70 mm was set rotatable with bearings between cisterns A and B. The cylinder and cisterns were filled with

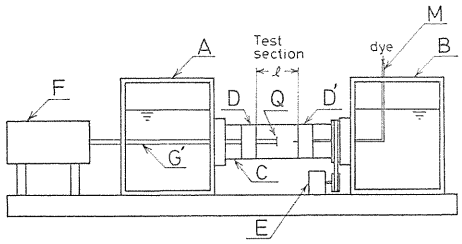

A, B: Cistern C: Cylinder D, D′: End plate E: DC motor
F: Disk driving mechanism M: Dye leading tube
Q: Oscillating disk

Fig. 1. 9. Experimental apparatus.

water. The cylindrical vessel consisted of the cylinder and end plates D, D′ with a thickness of 30 mm. The region in the vessel was a test section and its length l was freely adjusted. The cylinder was belt-driven by a variable speed DC motor E, so that a rigidly rotating flow field was induced in the test section. It is well known that the elastoid-inertia oscillation cannot be self-excited in such a flow field. In order to induce the oscillation, a small disk Q was set in the test section by a rod G′ and driven to oscillate in the axial direction by a mechanism F.

Details of the disk drive mechanism are shown in Figs. 1. 10 (a) to (c). The mechanism for axisymmetric mode ($s=0$), similar to the one of Fultz, is shown in Fig. 1. 10 (a). Sinusoidal motion with variable half stroke (0∼10 mm) and frequency (0. 2∼2Hz) was generated by a yoke cam mechanism and transmitted through the members G and G′. A circular disk of diameter 20 mm was fixed at

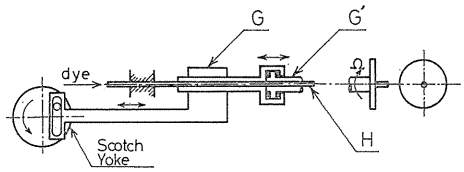

(a) $s=0$ mode.

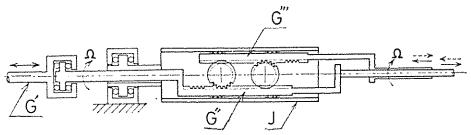

(b) $s=1$, 2 mode.

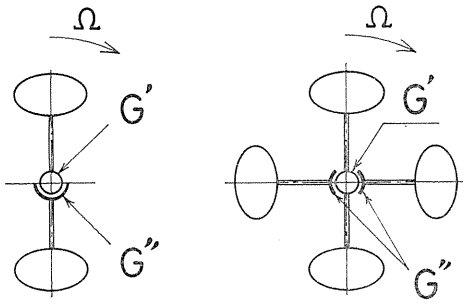

(i) $s=1$ (ii) $s=2$

(c) Arrangement of the disks.

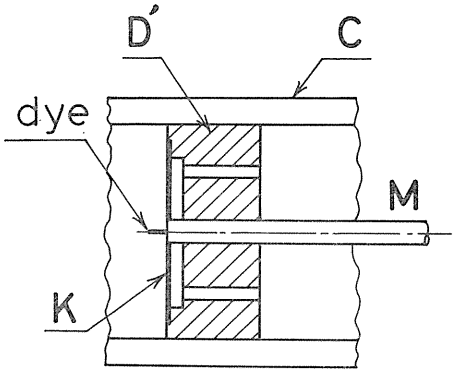

(d) End plate.

Fig. 1. 10. Details of disk driving mechanism and end plate.

the end of the member G′ which rotated with the cylinder while moving back and forth in the axial direction. Dye was injected at the center of the disk through a leading tube H of inside diameter 1 mm. The mechanisms for higher mode ($s=1$, 2) are shown in Fig. 1. 10 (b). Sinusoidal motion of G′ in the axial direction was transmitted to the member G″, and further to the member G‴ with a reversal of the phase through gears set in a casing J. These members rotate together with the cylinder as a unit. A pair (for $s=1$) or two pairs (for $s=2$) of elliptic disks with the major axis 15 mm and the minor axis 10 mm were fixed at some distance in the radial direction from the end of the members G″ and G‴ [Fig. 1. 10(c)].

In investigation of the flow field for each mode of the oscillation, the radial position and the phase of the axial oscillatory motion for each disk were determined as follows. The disk was fixed at a theoretically expected radial position where axial velocity fluctuation $\tilde{w}$ should be greatest for each mode of the oscillation [see Eq. (1. 6)]. For $s=1$ mode oscillation, a pair of disks were positioned opposite side each other [Fig. 1. 10 (c-i)]. The disks were oscillated with the reverse phase. For $s=2$ mode oscillation, two pairs of disks were positioned across each other [Fig. 1. 10 (c-ii)]. One pair of disks were oscillated with the reverse phase to the other pair.

A surface of the end plate D′ (see Fig. 1. 9) fronting the test section was constructed of a flexible plate K with thickness 0. 8mm, in order to absorb a small fluctuation of the section volume induced through the movement of the disk driving mechanism [Fig. 1. 10 (d)]. And a leading tube M was set along the axis through which dye was injected to visualize the flow field.

In the experiment the circular frequency n_f' of the forced oscillation by the rotating disks was varied in steps for the fixed value of the test section length l

and the rotatory angular velocity Ω. A resonance was observed at a certain frequency of oscillation while the flow field was visualized by means of dye injection or a depth tuft. Characteristics of the flow field in resonance were compared with the theoretical results of the elastoid-inertia oscillations. Resonance was distinguished by the following conditions for each mode of oscillation. In the resonant state of axisymmetric mode ($s=0$), a back and forth motion of dye injected on the axis coincides in phase with the disk motion and shows the greatest amplitude. For a higher azimuthal mode of the oscillation ($s=1, 2$) the characteristic flow, which can be theoretically expected, is observed most clearly in resonance near the center of the end plate by means of dye injection or a depth tuft.

Because the forced oscillation is induced by the disks rotating with the cylinder, the circular frequency n'_{fr} in resonance must be identical with the natural frequency $n'=n-s\Omega$ [cf. Eq. (1.8)] in the rotatory coordinate system. By reference to Eq. (1.9) the natural circular frequency n_e in the stationary system should be estimated as

$$n_e=n'_{fr}+s\Omega \tag{1.15}$$

The value of n_e is compared with the theoretically expected value n for the corresponding mode of oscillation.

1. 3. 2. Experimental Results and Discussions

1. 3. 2. 1. s=0 Mode (Axisymmetric Mode)

For the axisymmetric mode Fultz made an experimental study with an apparatus similar to the one in this study, showing that the natural frequency of the oscillation agreed well with the inviscid linear theory within an accuracy of 0.5~1%. And the characteristic flow pattern was observed in resonant state through flow visualization by means of dye injection. However detailed theoretical examination of the observed flow pattern could not be finded.

Here the flow pattern of axisymmetric mode is compared with the theoretical estimation. Figure 1.11 (a) shows a characteristic mushroomlike flow pattern visualized by dye injection in the resonant state. The flow was illuminated with a sheet of parallel light and photographed from the direction normal to it. A small amount of dye was injected continuously on the axis at $L/3$ distance from the end plate on the right side, while the disk was driven periodically with an amplitude of $L/6$ on the center of the axis ($L=l/a$; l test section length, a radius). With a disk motion, dye gradually spread in the test section under the influence of diffusion: the figure shows a visualized flow pattern at 17 minutes after the beginning of the dye injection. Other parameter values, namely rotational angular velocity Ω, dimensions of the test section, half stroke A_f and circular frequency n_e of the disk motion are given in the figure.

The flow field in the same geometry as the experiment for (0, 1, 1) mode oscillation is described in Figs. 1.11 (b) to (d) as the projection of pathlines onto R-Z plane. Pathlines of eight fluid particles arranged in a circle of radius $R=0.2$ at an axial distance $Z=L/3$ are obtained in a period of oscillation from Eq. (1.13). The pathlines in Fig. 1.11 (b) show a complicated pattern in comparison with the one of streamlines in Fig. 1.3. This figure, however, gives only a qualitative explanation of the chacteristic flow, because an extremely large amplitude ($C=2.5$) is assumed in the calculation.

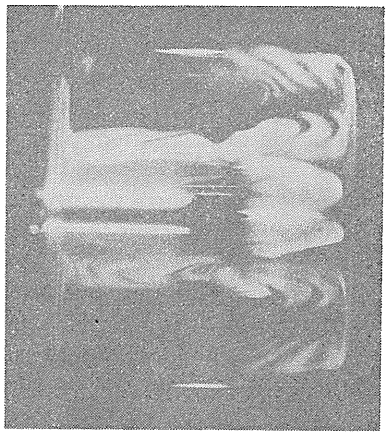

(a) Photograph for (0, 1, 1) mode oscillation.
l=60mm, a=35mm (L=1.714)
Ω=2.58rad/s, n_e=2.23rad/s (N=0.86)
A_f=9.5mm (C=0.24)

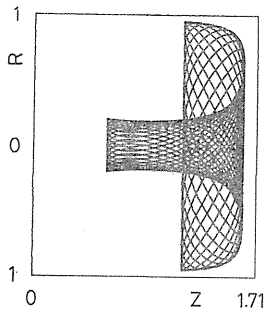

(b) Calculated pathlines.
L=1.714, M=1.833,
N=0.863, C=2.5

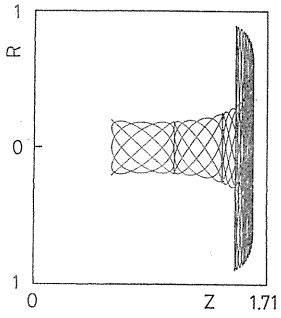

(c) L=1.714, M=1.833,
N=0.863, C=0.238,
T=30.0

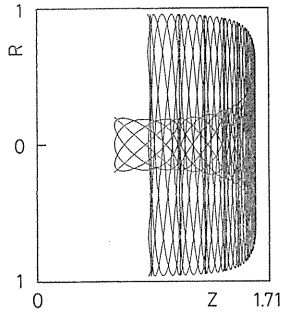

(d) L=1.714, M=1.833,
N=0.863, C=0.238,
T=45.0

Fig. 1. 11. Visualized flow pattern of axisymmetric oscillation (s=0) and corresponding calculations.

In Figs. 1.11 (c) and (d), on the other hand, the amplitude of fluctuation C is determined from a half stroke A_f of the disk oscillation in the experiment as

$$C=nA_f/a\Omega$$

where n is dimensionless circular frequency, and a is radius. In the above calculation the effect of diffusion (to the right side) is estimated as follows. Pathlines are drawn with the fluctuation amplitude mentioned above, then the next step pathlines are sought from the farthest point within reach of particles. By repetition of this procedure Figs. 1.11 (c) and (d) are obtained. The flow pattern of the latter shows good agreement with the experimental result [Fig. 1.11 (a)]. The above investigation suggests that the elastoid-inertia oscillation in a real fluid under the influence of viscosity and nonlinearity can be well estimated in its flow pattern by the inviscid linear theory.

1. 3. 2. 2. s=1 mode

A remarkable characteristic in s=1 mode oscillation is recognized in Fig. 1.2

showing the relation between natural circular frequency N and test section length L. A steady flow in the stationary coordinate system can exist for (1, 1, 1) mode oscillation: for $L=1.99$ ($L=l/a$) the natural circular frequency N ($=n/\Omega$) reduces to 0, which means that the velocity field becomes independent of time T. We refer to the flow for $N=0$ as "stationary elastoid-inertia oscillation." The flow field of the $s=1$ mode oscillation was examined from this viewpoint.

Figure 1.12 (a) shows the calculated streamlines for the stationary oscillation viewed from a direction making an angle of 60° with Z-axis. Circular streamlines

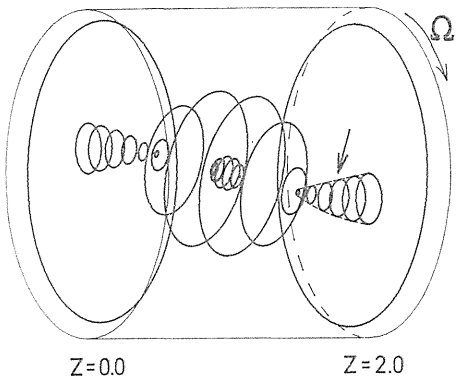

(a) Steady streamlines in stationary system.
$L=1.99$, $M=1.58$, $N=0$, $C=0.2$

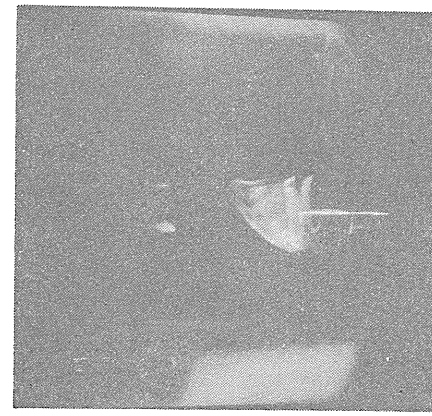

(b) Visualized cone shape.
$l=69.6$mm, $a=35$mm, ($L=1.99$)
$\Omega=2.86$rad/s, $|n_f'|=2.83$rad/s
($|N_f'|=0.99$), $A_f=5$ mm

Fig. 1. 12. Flow pattern for stationary oscillation of $s=1$ mode.

near the end plates are arranged along the swirling axis (which is different from the cylinder axis), whose envelope takes on a cone shape. The corresponding flow pattern was observed also in the experiment. Stationary cone near the end plate was visualized by dye injection, when the circular frequency of the forced oscillation was adjusted at $|n_f/\Omega|=0.99$ corresponding to $N=0.01$ for the test section of its length $L=1.99$. The resonance is quite sensitive to the frequency n_f in the rotatory coordinate system. The shape of the cone breaks down with a small change of frequency (about 1 %).

For the other case of $s=1$ mode oscillations ($N\neq 0$), helix shape streaklines were observed in good agreement with theoretically expected configurations.

1. 3. 2. 3. $s=2$ Mode

The flow field of $s=2$ mode oscillation never assumes a steady state. The behavior of fluid particles visualized by dye injection was examined in comparison with the theoretical results.

A sample of calculation is shown in Fig. 1.13 (a). Fluid particles are initially placed on the end plate ($Z=L$) in concentric circles with three different radii, namely $R=0.05$, 0.1, 0.2, being apart from each other at an angle of 6° [Fig. 1.13 (a) (i)]. Particles deviate to form a slender configuration [Fig. 1.13 (a) (ii)]

evolving into a pattern like the letter "S" with the passage of time [Figs. 1. 13 (a) (iii) and (iv)].

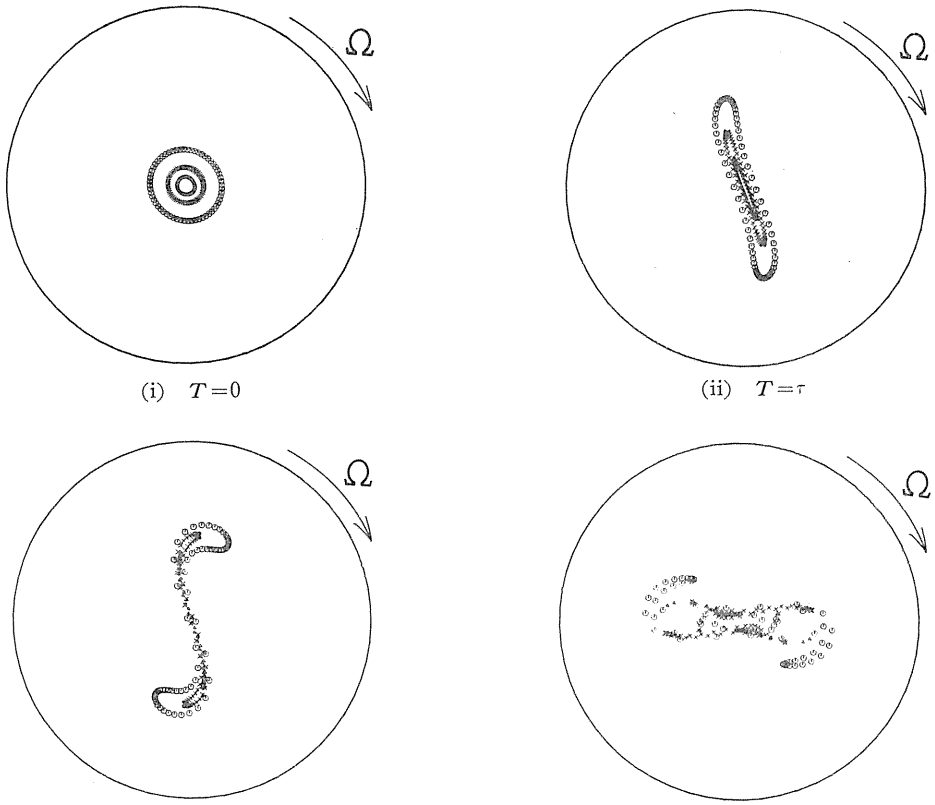

(i) $T=0$ (ii) $T=\tau$

(iii) $T=2\tau$ (iv) $T=5.5\tau$

(a) $L=3$, $M=1.047$, $N=1.559$, $(N'=-0.441)$, $C=0.24$, $\tau=2\pi/N=4.03$

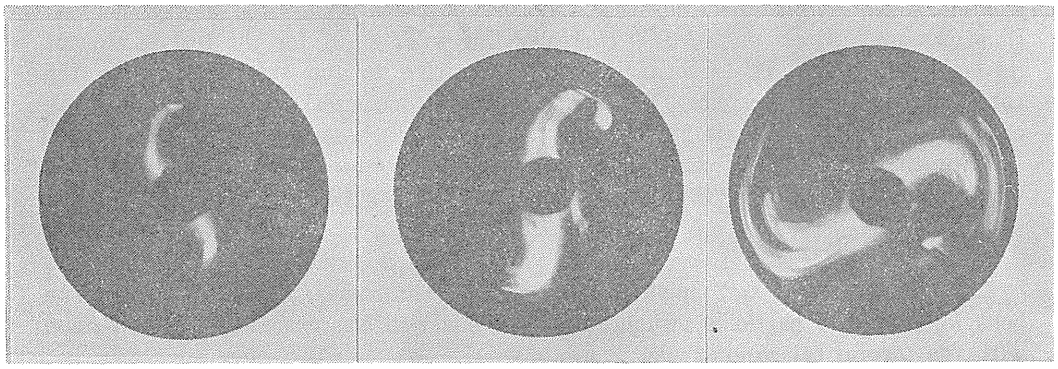

(1) $t=14$s (2) $t=34$s (3) $t=54$s

(b) $l=105$mm, $a=35$mm, $(L=3.0)$, $\Omega=3.17$rad/s, $|n_e'|=1.38$rad/s, $(|n_e'/\Omega|=0.437)$, $A_f=9.5$mm $(C=0.24)$

Fig. 1. 13. Dye region deformation due to $s=2$ mode oscillation.

Resonance was noted when visualized fluid particles showed a characteristic flow pattern corresponding to the above results. Figure 1.13 (b) shows the successive deformation of dye visualized region in the same condition as the calculation ($L=3.0$, $C=0.24$), where the dark circular portion at the center of each photograph is a shadow of dye leading tube. The flow patterns show good agreement with the theoretical results except for the time elapsed.

Measured values of natural circular frequencies for each mode ($s=0$, 1, 2) are shown in Fig. 1.2 by circular symbols. For $s=1$ mode a resonance could not be sharply distinguished except for the stationary oscillation ($N=0$): the observed resonance range is indicated by a segment between the circular symbols. These results prove that the inviscid linear theory gives a good estimation of the natural frequency for several mode oscillations.

1. 4. Conclusions

In this chapter experiments are performed on the elastoid-inertia oscillations, for which expressions are known through the inviscid linear theory but the flow field of real fluid has not been clarified. The experimental results prove that the inviscid linear theory gives a qualitatively good estimation of the oscillation both in the flow pattern and in its natural frequency including the higher azimuthal modes ($s=1$, 2).

These results suggest the propriety of an approach from the linear theory to many hydraulic problems which are supposed to involve inertial waves: for example, vortex breakdown phenomena in circular pipe or on delta wings, precessional motion of vortex in cyclone separator, vibrations in draft tube of water turbine and vortex whistle in swirling pipe flow.

2. Vortex Breakdown Phenomena of Stationary Type

2. 1. Introduction

An abrupt change in flow structure can occur at some place along the axis in a swirling flow when the azimuthal velocity is relatively large as compared with the axial velocity. Such phenomena, called the vortex breakdown, were first observed by Peckham and Atkinson[9] on delta wings at large incidences. Since then, many experimental investigations have been made, early ones by Lambourne[10] and Hummel[11] on breakdown over wings, and later ones on the phenomena in a swirling pipe-flow. Theoretical investigations have also been made by Squire, Benjamin,[12] Ludwieg,[13] Hall,[14] Bossel,[15] Leibovich,[16] Randall,[17] Grabowski[18] and others.

Sarpkaya[19] found in his detailed experiments on the phenomena in a slightly divergent pipe, that vortex breakdowns occur in three different types: (1) axisymmetric (bubble type), (2) spiral and (3) double helix (triangular sheet type). In addition, Leibovich[20] observed six distinct types of breakdown occurring in a pipe similar to Sarpkaya's.

As mentioned above, there are many reports on the vortex breakdown, but due to complexity and variety of flow structure of breakdown, most of theoretical investigations are limited mainly to the axisymmetric type. And any does not give a reasonable explanation for the occurrence of various types of breakdown. There remain a lot of essential features of the phenomena to be clarified.

The aim of the present study is to give a theoretical explanation for the vortex breakdown phenomena of the swirling flow in a circular pipe. It is found that the internal wave (inertial wave), which may occur in the swirling flow, plays the significant role in the breakdown phenomena, and that the azimuthal modes of the wave correspond directly to distinct types of flow structures which include the three types of Sarpkaya and also six types of Leibovich.

In this chapter, the investigation is limited to time-independent (stationary) types of the phenomena, and the time-dependent (unsteady or periodic in time) types will be discussed in next chapter.

2. 2. Inertial Waves (Wave Disturbances) in Swirling Pipe Flow

After the time when Kelvin's report[3] was presented, it has been well known that an inertial wave can occur in a swirling flow field. Sorberg and Bjerkness,[4] Long,[6] and Fultz[8] treated the wave in respective cases of rotating flow. In the following, the wave disturbances (fluctuations) are investigated with a view to examining the relation between those and the vortex breakdown phenomena in a circular pipe.

2. 2. 1. Basic Equations for Wave Disturbances

For analyzing the wave disturbances occurring in the swirling flow within a circular pipe, cylindrical polar coordinates (r, θ, z) are introduced as shown in Fig. 2. 1. In the analysis the following is assumed: (1) Fluid is inviscid and incompressible. (2) Primary flow (flow before disturbance occurs) is cylindrical and the velocity components are $\overline{W}(r)$ and $\overline{V}(r)$, where the azimuthal velocity $\overline{V}(r)$ and the axial velocity $\overline{W}(r)$ are arbitrary functions of radius r. (3) The velocity variations are small amounts in comparison with $\overline{V}(r)$ and $\overline{W}(r)$ of primary flow. From the assumption (1), Euler's equations of motion and continuity equation are taken as the fundamental equations governing the fluid motion. From the assumption (2), the primary flow is expressed as follows:

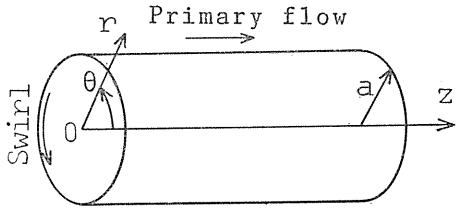

Fig. 2. 1. Coordinate system.

$$\bar{u}=0, \quad \bar{v}=\overline{V}(r), \quad \bar{w}=\overline{W}(r), \quad \bar{p}/\rho=(\bar{p}_0/\rho)+\int_0^r (\overline{V}(r)^2/r)\,dr \qquad (2.1)$$

where u, v and w are the velocity components on coordinates r, θ and z; p is the pressure and p_0 is the pressure at the axis of a pipe (over-bar denotes the primary flow component). The velocity components of the flow field involving the disturbances are expressed as the sum of both the primary flow and the disturbance components, and can be described in the following form.

$$\left.\begin{aligned} &\tilde{u}=\bar{u}+\tilde{u}=U(r)\,e^{-i(s\theta+mz)+\lambda t}, \quad v=\bar{v}+\tilde{v}=\overline{V}(r)+V(r)\,e^{-i(s\theta+mz)+\lambda t} \\ &w=\bar{w}+\tilde{w}=\overline{W}(r)+W(r)\,e^{-i(s\theta+mz)+\lambda t}, \\ &p=\bar{p}+\tilde{p}=\bar{p}_0+\rho\int_0^r (\overline{V}^2/r)\,dr+P(r)\,e^{-i(s\theta+mz)+\lambda t} \end{aligned}\right\} \qquad (2.2)$$

where $U(r)$, $V(r)$, ... are complex functions of r (hereafter denoted simply by U, V, ...), λ is a complex number, m is a real number, and s is a positive integer (including zero). The tilde~ indicates components of the disturbances. Introducing Eq. (2.2) into the fundamental equations, following set of linear equations (2.3) can be obtained. Further in the induction of above equations, the expressions (2.1) and assumption (3) are taken into consideration.

$$U\{\lambda-(is\bar{V}/r)-im\overline{W}\}-2(\bar{V}/r)V=-(1/\rho)\left(\frac{dP}{dr}\right) \tag{2.3.a}$$

$$V\{\lambda-(is\bar{V}/r)-im\overline{W}\}+\left\{\left(\frac{d\bar{V}}{dr}\right)+(\bar{V}/r)\right\}U=(1/\rho)(is/r)P \tag{2.3.b}$$

$$W\{\lambda-(is\bar{V}/r)-im\overline{W}\}+\left(\frac{d\overline{W}}{dr}\right)U=(1/\rho)imP \tag{2.3.c}$$

$$\left(\frac{dU}{dr}\right)+(1/r)U-(is/r)V-imW=0 \tag{2.3.d}$$

The solution of the above equations which satisfies a boundary condition at the pipe wall, describes a wave disturbance that occurs in the swirling flow.

2. 2. 2. Neutrally Stable Disturbance in Rigidly Rotating Flow with Uniform Axial Velocity and Perturbed Flow Field

It is difficult to solve Eqs. (2.3) analytically. To facilitate the analytical treatment, two assumptions are added: [1] The primary flow is rigidly rotating with uniform axial velocity, that is,

$$\bar{V}(r)=\Omega r, \quad \overline{W}(r)=W_0=\text{constant} \tag{2.4}$$

Indeed, it is seen in many experimental studies that the azimuthal velocity $V(r)$ in the vicinity of the pipe axis, is close to a rigid rotation profile (constant angular velocity Ω: $\Omega>0$). [2] The disturbance is limited to a neutral stable wave, i. e., when λ is written as

$$\lambda=\alpha+in \tag{2.5}$$

only the case of $\lambda=in$ ($\alpha=0$, n: real) is considered. Under the assumptions [1] and [2], Eqs. (2.3) can be simplified, and the equation with respect to W alone is derived after elimination of other variables in the following Bessel's equation form.

$$\frac{d^2W}{dr^2}+\frac{1}{r}\frac{dW}{dr}+W\left[\frac{m^2\{4\Omega^2-(n-s\Omega-m\overline{W}_0)^2\}}{(n-s\Omega-m\overline{W}_0)^2}-\frac{s^2}{r^2}\right]=0 \tag{2.6}$$

W is generally a complex function, but in this case the real function W_R ($W=W_R+iW_I$) satisfies the same equation as Eq. (2.6). Then, hereafter W indicates a real function. (U, V and P also represent real functions.) Now, from the solution of Eq. (2.6), after several calculations the real solution of the neutrally stable disturbance can be expressed in the following form.

$$\left.\begin{aligned}\tilde{u}=U\sin(nt-s\theta-mz)=A\frac{m}{\sigma}\Big[J_{s-1}(\sigma r)\\ -\Big\{\frac{2\Omega+(n-s\Omega-mW_0)}{(n-s\Omega-mW_0)}\Big\}\Big(\frac{s}{\sigma r}\Big)J_s(\sigma r)\Big]\sin(nt-s\theta-mz)\end{aligned}\right\} \quad (2.7.\text{a})$$

$$\left.\begin{aligned}\tilde{v}=V\cos(nt-s\theta-mz)=\frac{A}{\sigma}\frac{m}{(n-s\Omega-mW_0)}\Big[2\Omega J_{s-1}(\sigma r)-\\ \Big(\frac{s}{\sigma r}\Big)\{2\Omega+(n-s\Omega-mW_0)\}J_s(\sigma r)\Big]\times\cos(nt-s\theta-mz)\end{aligned}\right\} \quad (2.7.\text{b})$$

$$\tilde{w}=W\cos(nt-s\theta-mz)=AJ_s(\sigma r)\cos(nt-s\theta-mz) \quad (2.7.\text{c})$$

$$\frac{\tilde{p}}{\rho}=\frac{P}{\rho}\cos(nt-s\theta-mz)=A\frac{(n-s\Omega-mW_0)}{m}J_s(\sigma r)\cos(nt-s\theta-mz) \quad (2.7.\text{d})$$

where A is an arbitrary constant indicating the amplitude of disturbance, J_s is an sth-order Bessel function of the first kind; and σ is thus defined:

$$\sigma=[m^2\{4\Omega^2-(n-s\Omega-mW_0)^2\}/(n-s\Omega-mW_0)^2]^{1/2} \quad (2.8)$$

The value of σ is determined from the following eigenvalue equation, which is introduced with the boundary condition $u=0$ at the pipe wall.

$$J_{s-1}(\sigma a)/J_s(\sigma a)=(s/\sigma a)\{1\pm\sqrt{1+(\sigma/m)^2}\} \quad (2.9)$$

where a is the pipe radius. For each one of double sign in the above equation, it is found that there exists an infinite number of positive eigenvalue $\sigma_{\pm g}(g=1, 2, 3\ \ldots)$ [$+g$ or $-g$ indicates an eigenvalue of the gth order respectively for positive or negative sign in Eq. (2.9)].

Expressions (2.7.a)$\sim$(2.7.d) indicate the wave motion propagating in both the axial and azimuthal directions, and signify the inertial wave occurring in the primary swirling flow field. The wave propagating downstream (in the direction of positive z) or upstream is referred to as a forward or a backward progressive wave, respectively. According to the positive or negative values of m and n, the propagating modes of the wave are determined as follows. (1) $m>0$, $n>0$: forward progressive wave with a positive azimuthal phase velocity. (2) $m>0$, $n<0$: backward progressive wave with a negative azimuthal phase velocity. (3) $m<0$, $n>0$: backward progressive wave with a positive azimuthal phase velocity. (4) $m<0$, $n<0$: forward progressive wave with a negative azimuthal phase velocity. These waves have an azimuthal phase velocity equal to n/s in the z section. When $s=0$, the wave becomes an axisymmetric disturbance which propagates only in the z direction. The flow field involving the wave disturbance is expressed as follows.

$$u=\tilde{u},\quad v=\Omega r+\tilde{v},\quad w=W_0+\tilde{w},\quad (p/\rho)=(\bar{p}_0/\rho)+(1/2)\Omega^2r^2+(\tilde{p}/\rho) \quad (2.10)$$

2. 2. 3. Wave Disturbance with no Phase Velocity (Stationary Wave)

The disturbance expressed by Eqs. (2.7) signifies a progressive wave (in gene-

ral $n/m \neq 0$, $n/s \neq 0$). However, if $n=0$, it becomes a disturbance resting in the coordinates or fixed in the space (referred to as a stationary wave). The expression of stationary wave is obtained as follows [c. f., Eqs. (2.7)].

$$\tilde{u}=C\frac{m}{\sigma}\left[J_{s-1}(\sigma r)+\frac{\{2\Omega-(s\Omega+mW_0)\}}{(s\Omega+mW_0)}\left(\frac{s}{\sigma r}\right)J_s(\sigma r)\right]\sin(s\theta+mz) \quad (2.7.a)'$$

$$\tilde{v}=\frac{C}{\sigma}\frac{m}{(s\Omega+mW_0)}\left[2\Omega J_{s-1}(\sigma r)-\left(\frac{s}{\sigma r}\right)\{2\Omega-(s\Omega+mW_0)\}J_s(\sigma r)\right]\cos(s\theta+mz) \quad (2.7.b)'$$

$$\tilde{w}=-CJ_s(\sigma r)\cos(s\theta+mz) \quad (2.7.c)'$$

$$\frac{\tilde{p}}{\rho}=C\frac{(s\Omega+mW_0)}{m}J_s(\sigma r)\cos(s\theta+mz) \quad (2.7.d)'$$

where $C=-A$. As mentioned before, this study concerns the time-independent type of vortex breakdown, so the above stationary wave is mainly discussed in the following.

The equations and expressions introduced so far, are nondimensionalized by taking the representative length and time as the pipe radius a and Ω^{-1}. Main nondimensional quantities are: $R_o=W_0/a\Omega$, $M=am$, $N=n/\Omega$, $\sigma'=a\sigma$, $T=\Omega t$, $A'=A/a\Omega=-C/a\Omega$, R_o indicates the Rossby number. Now, from Eq. (2.8), N is written as

$$N=s+MR_0\pm 2\sqrt{M^2/(M^2+\sigma'^2)} \quad (2.8)'$$

where the double sign corresponds to that in Eq. (2.9). Though there exists an infinite number of values of σ' in the above equation, only the least order of σ' (σ_1' or σ_{-1}') is here taken into account because it is inferred that most phenomena appear dominantly in the mode of the least order.

First, the case of σ_1' is considered. From Eq. (2.8)', the inequality $N/M>R_o$ always holds for $M>0$. Hence the stationary wave cannot exist for $M>0$. However, it can exist for $M<0$. Figure 2.2 shows the above relation, which plots the nondimensional angular frequency N of the disturbance against the nondimensional wave length of the axial direction $L_z(=\lambda/a)$. Figures (a), (b) and (c) correspond to the parameter $s=0$, 1, 2, respectively. The parameter s signifies the azimuthal mode of the disturbance. Broken lines and chain lines in the figures represent the cases of $M>0$ and $M<0$, respectively. The curves are calculated for different values of the Rossby number. The curves for $R_o=0$ is shown by a solid line. (In this particular case N does not depend on the sign of M.) The intersecting point of the calculated curve and the abscissa $N=0$, signifies the stationary wave. As seen in the figure, in case of σ_1', the stationary wave can exist only for $M<0$.

When σ_{-1}', which corresponds to the negative sign in Eq. (2.8)' is considered, the calculated curves take a form close to the mirror image of those in Figs. (a), (b) and (c) with respect to the lines $N=0$, 1, 2, respectively. The curves for $s=1$ are shown in Fig. (d). From the results concerning σ_{-1}' it is known that there is a range of L_z where the stationary wave of $s=0$, 1 can exist even for $M>0$, but the stationary wave of $s=2$ cannot exist for $M>0$.

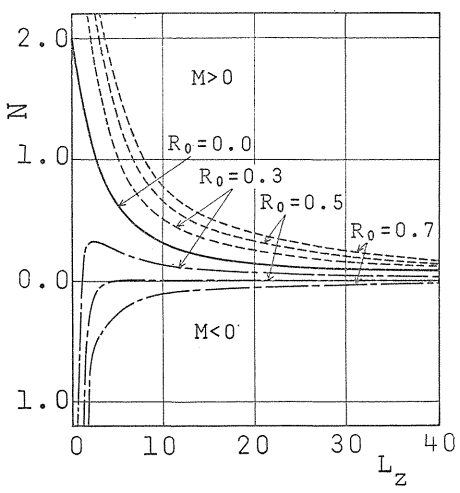

(a) σ_1', $s=0$

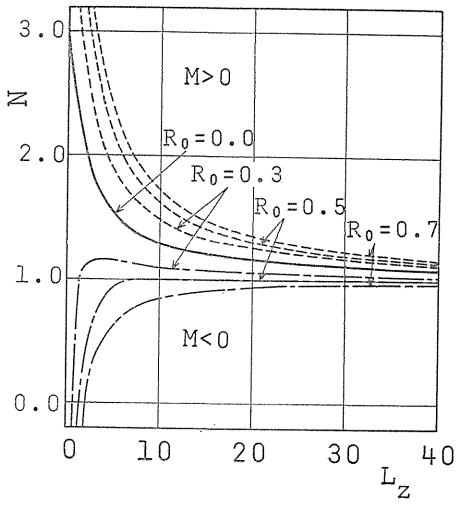

(b) $s=1$

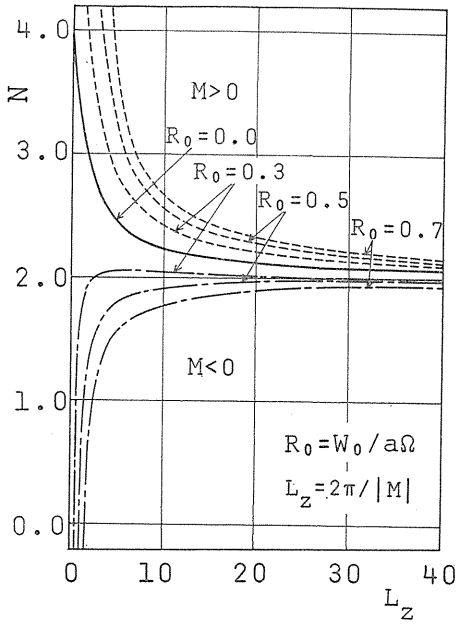

(c) $s=2$

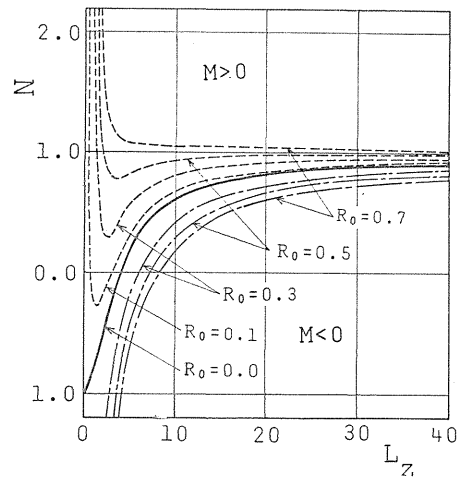

(d) σ_{-1}', $s=1$

Fig. 2. 2. Angular frequency N of wave disturbance versus nondimensional wave length L_z.

Several properties of the stationary wave are described in the following. Equation (2. 8)′ gives

$$(N/M)_{R_0=0}=\frac{1}{M}\left[s\pm 2\sqrt{M^2/(M^2+\sigma'^2)}\right]$$

where $(N/M)_{Ro=0}$ indicates the axial phase velocity of the disturbance in the swirling flow with no mean axial velocity (i. e., $W_0=0$). The above equation and Eq. (2. 8)′ for $N=0$ yield

$$(N/M)_{Ro=0}=-R_0 \tag{2. 11}$$

which is rewritten in the dimensional form as

$$(n/m)_{W_0=0}=-W_0 \tag{2. 11)′}$$

This means that when the stationary wave occurs, the relative upstream velocity of the disturbance is equal to the mean axial velocity, so that the wave remains fixed in the space.

The following result is obtained with regard to a condition of the existence of the stationary wave. From Eq. (2. 8)′ it follows for $s=0$ that,

$$R_0=2/\sqrt{M^2+\sigma'^2} \tag{2. 12}$$

And then the eigenvalue equation (2. 9) reduces to $J_1(\sigma')=0$, which gives σ' equal to 3. 83 (as the least order of the value). Therefore the range of the existence of the stationary wave for $s=0$ is

$$0<R_0(=W_0/a\Omega)<0.522 \tag{2. 13}$$

Hence the axisymmetric mode of the stationary wave is possible for a Rossby number less than a constant value. However, in case of the non-axisymmetric mode of the stationary wave ($s=1$, 2), there is no restriction on the Rossby number, because for any Rossby number the value of M can be determined such as to give $N=0$ [c. f., Eqs. (8)′, (9)′ and Fig. 2. 2]. It should be noted that the flow field involving the stationary wave, becomes a steady flow.

2. 3. Stationary Wave and Stationary Vortex Breakdown

In this section, it is shown that the swirling flow involving the stationary wave as a disturbance, is in a good agreement in its pattern with the observed time-independent (stationary) breakdown.

As mentioned before, Sarpkaya[19] identified three distinct types of breakdown from his experimental results which are obtained by visualization technique with dye; i. e., (1) axisymmetric-bubble, (2) spiral and (3) double helix. Moreover, Leibovich[20] reported that 6 different types of breakdown exist and called them as type 0 ~ type 6. Type 0, 2 and 5 are almost the same as Sarpkaya's bubble, spiral and double helix types, respectively. In addition, there are new types 3, 4 and 6. (Type 1 is a deformed one of type 0). Type 6 indicates that the central fluid filament moves off axis at a certain position and curves into a gentle spiral with the same sense as the rotating direction of the primary flow; type 4 forms a flattened bubble, and in type 3 the central dye filament (at the inlet of pipe, it coincides with the pipe axis) moves abruptly off axis with a sharp kink, oscillating from side to side in a preferential plane. Leibovich pointed out that among these types, only type 5 and type 6 are purely stationary (that is, the streamlines visualized with the dye remain steady and fixed in the space). In this chapter type 0 (approximately stationary) and type 5 and 6 are mainly discussed, and type 4 is briefly treated. Type 2, which is unsteady and temporally periodic, and type 3,

which seems to be related with type 2, are excluded here (They are discussed in the next chapter).

As will be mentioned in section 4, it is considered that the vortex breakdown has a close relationship with the wave disturbance which comes from the instability of the mean flow. This paper does not treat the stability problem of the disturbance, but describes the structural modes of the breakdown, especially those of the stationary types. Hence, a neutrally stable wave disturbance is adopted to calculate the flow pattern of the flow field involving the disturbance. In addition, in spite of the assumption of small disturbance, the magnitude of the amplitude (A') of the disturbance is taken as the order of unity to calculate streamlines or velocity profiles of the flow field. The result can be considered to give an approximate model for the final state of breakdown, which may be affected by the nonlinearity of fluid motion after a small disturbance grows up.

2. 3. 1. Axisymmetric Mode ($s=0$) of Stationary Wave and Bubble Type (Type 0) Breakdown

The breakdown of the Leibovich's type 0, which exhibits an axisymmetric bubble at a position on the swirling axis, is closely related to the occurrence of the stationary wave of $s=0$ type. The velocity components u, v and w for $s=0$ mode disturbance can be easily obtained from Eqs. (2. 7)′ and (2. 10). The equation for the streamline is written in the following dimensional form.

$$dr/u=rd\theta/v=dz/w \tag{2. 14}$$

Figure 2. 3 (a) shows the streamlines calculated by computer by integrating the above equation for $s=0$. In the calculation the stationary wave is assumed to exist

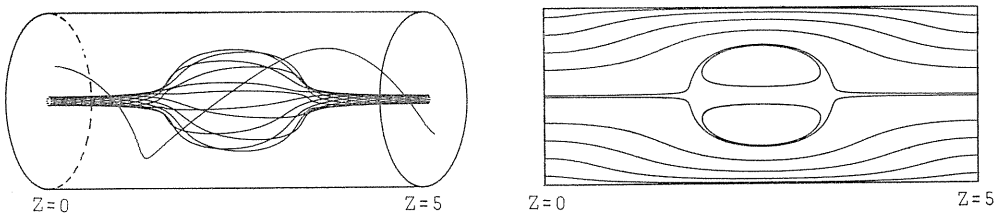

(a) Streamlines of $s=0$ mode. (b) Sectioned-streamlines of $s=0$ mode.

Fig. 2. 3. $s=0$ mode of stationary breakdown.
($R_0=0.496$, $M=-1.26$, $\sigma'=3.83$, $A'=-1.0$)

in the range of $Z>0$ ($Z=z/a$). $Z=0$ means the upstream boundary of the figure. The figure shows 12 streamlines which surround the pipe axis at the upstream end with a small circle of the radius $R=r/a=0.01$, and a streamline off axis by $R=0.3$. Figure 2. 3 (b) shows the intersecting lines of the axisymmetric stream-surfaces and a plane including the pipe axis, that is, the curves (referred to as sectioned-streamlines) obtained by integrating the following equation with $\theta=$ const.

$$dr/u=dz/w \tag{2. 14}'$$

Both figures (a) and (b) indicate the occurrence of an axisymmetric bubble. Figure (a) explains qualitatively the results of the views by Sarpkaya, Ikeda[21] and Leibovich, those visualized the flow with dye. Figure (b) agrees well with the streamlines given by Nakamura,[22] measuring with a laser doppler anemometer. Figure 2.4 gives the velocity components $\mathbb{U}$, $\mathbb{V}$ and $\mathbb{W}$($\mathbb{U}=u/a\Omega$, $\mathbb{V}=v/a\Omega$, $\mathbb{W}=w/a\Omega$) at several Z sections [from Eqs. (2.7)′, (2.10)]. The position $Z=2.5$ corresponds to the center of the vortex bubble. Figure 2.4, especially Fig. (c), explains well an rapid deceleration near the front edge of the bubble, the stagnation and the reversal flow in the bubble. Thus the features of the phenomena, which have been experimentally observed, are obtained in spite of the fact that the assumptions under which Eqs. (2.7)′, (2.10) are derived differ to some extent from the situation of actual flow. Moreover, the variation of $\mathbb{W}$ profile in the Z direction also agrees well with the experimental result by Nakamura, except in the vicinity of the pipe wall. Therefore, it is seen that the occurrence of the stationary wave for $s=0$ adequately represents the axisymmetric bubble type (type 0) of the breakdown phenomena. It is noted that the vortex bubble shown in Fig. 2.3, appears to be periodic along the axis, which is seen from Eqs. (2.7)′. In most cases, the successive bubble does not occur in the actual swirling flow because once a vortex bubble develops, the flow field is largely disturbed in the wake of it. Thus only one bubble is shown in the figure. However, a few observers have reported a second bubble which occurs after the first one.

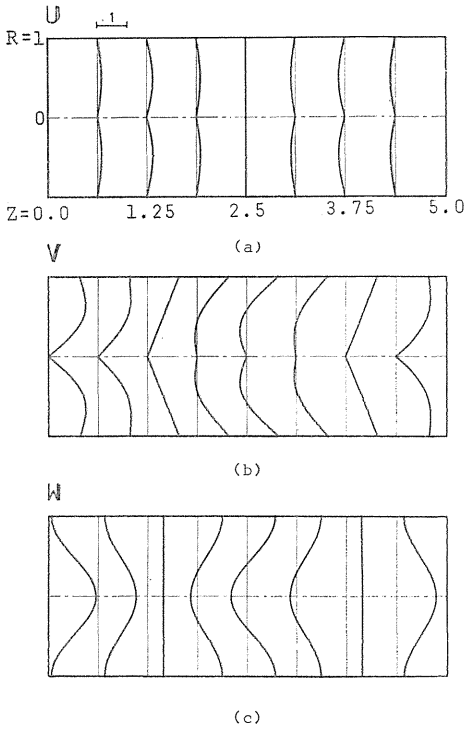

Fig. 2.4. Velocity component profiles of perturbed flow field given in Fig. 2.3.

2.3.2. *Non-axisymmetric Modes of Stationary Wave and Types of Breakdown*

In this section it is shown that the flow field in which the $s=1$ or $s=2$ mode of stationary wave occurs, exhibits the stationary, spiral type (type 6) or double helix type (type 5) vortex breakdown, respectively. Figure 2.5 shows a calculated result of the streamlines for $s=1$ [from Eqs. (2.7)′, (2.10), (2.14)]. It draws 6 streamlines surrounding the axis at $Z=0$ (i. e., at the upstream end of the stationary wave region). Figure (a) shows a view perpendicular to the axis, and Fig. (b) one from the downstream side. The streamlines which start from the center of a pipe section deflect off the axis, and form a gentle spiral, which shows good agreement with the visualized flow pattern of the type 6 breakdown of Leibovich. Figure 2.6 presents the sectioned-streamlines [from Eq. (14)′ for $\theta=0$, $(\pi/4)$, $(\pi/$

2)], and Fig. 2.7 shows the velocity profile in the same manner as Fig. 2.4 for $s=0$.

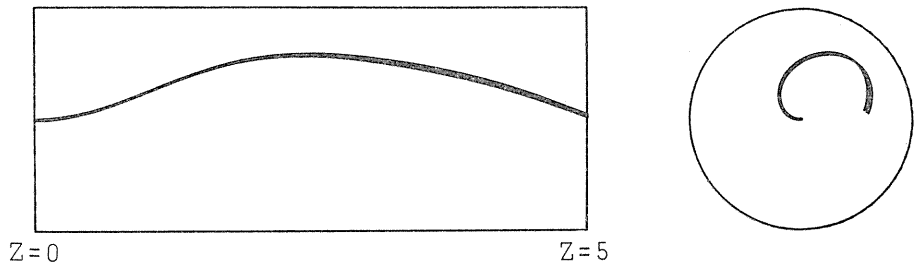

$R_0=1.31$, $M-1.12$, $\sigma'=4.61$, $A'=1.0$

Fig. 2. 5. Streamlines of stationary breakdown of $s=1$ mode.

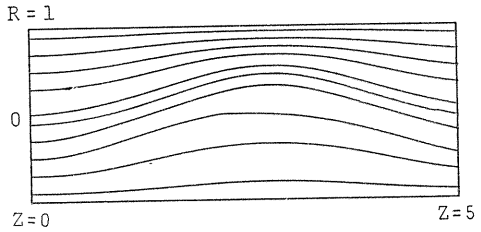

(a) Sectioned-streamlines by $\theta=0$ plane.

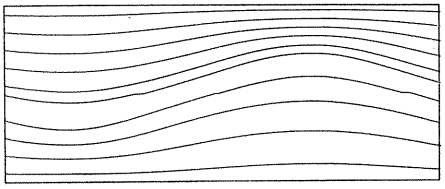

(b) Sectioned-streamlines by $\theta=\pi/4$ plane.

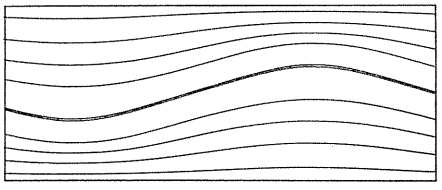

(c) Sectioned-streamlines by $\theta=\pi/2$ plane.

Fig. 2. 6. Sectioned-streamlines of $s=1$ mode.
(same conditions as Fig. 2. 5.)

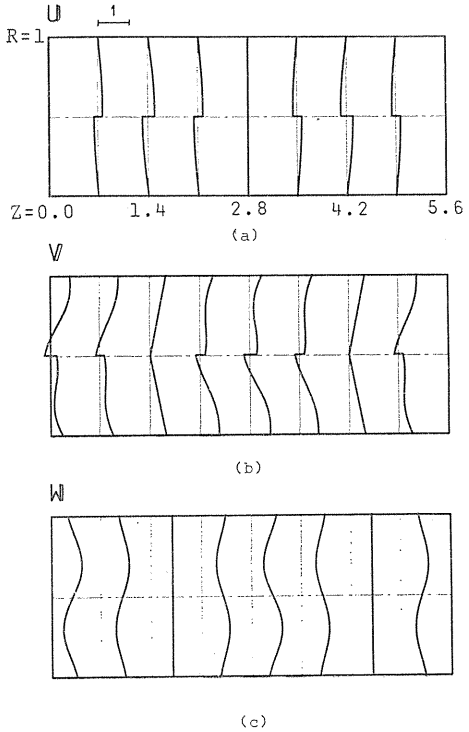

Fig. 2. 7. Velocity component profiles of $s=1$ mode.
(same conditions as Fig. 2. 5.)

Figure 2.8 shows the calculated streamlines for $s=2$. As seen in the figure, the central streamlines (12 lines) expand into a slightly twisted sheet, both edges of which envelop each other and form a double helix. This agrees well with the double helix type breakdown observed by Sarpkaya, Ikeda and Leibovich. In the figure the 12 fluid elements which passed through the upstream end ($Z=0$) at the same time, are denoted by ■ at time t_1 and by □ at time $t_2(t_2>t_1)$. These indications show more clearly that the streamlines expand into a sheet and form a

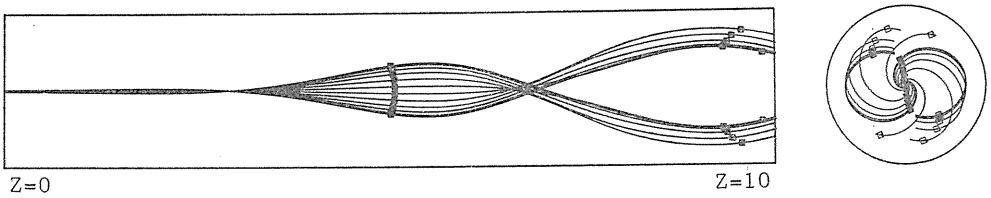

$R_o=1.5$, $M=-1.71$, $\sigma'=5.80$, $A'=-1.0$

Fig. 2. 8. Streamlines of stationary breakdown of $s=2$ mode.

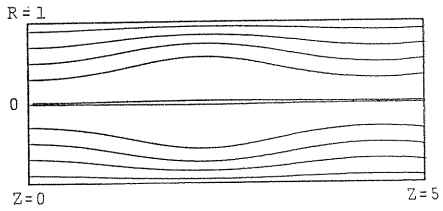

(a) Sectioned-streamlines by $\theta=0$ plane.

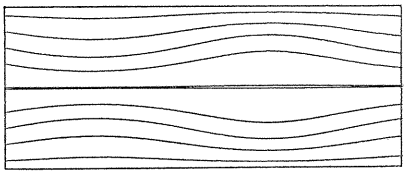

(b) Sectioned-streamlines by $\theta=\pi/4$ plane.

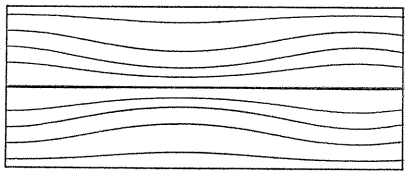

(c) Sectioned-streamlines by $\theta=\pi/2$ plane.

Fig. 2. 9. Sectioned-streamlines of $s=2$ mode.
(same conditions as Fig. 2. 8.)

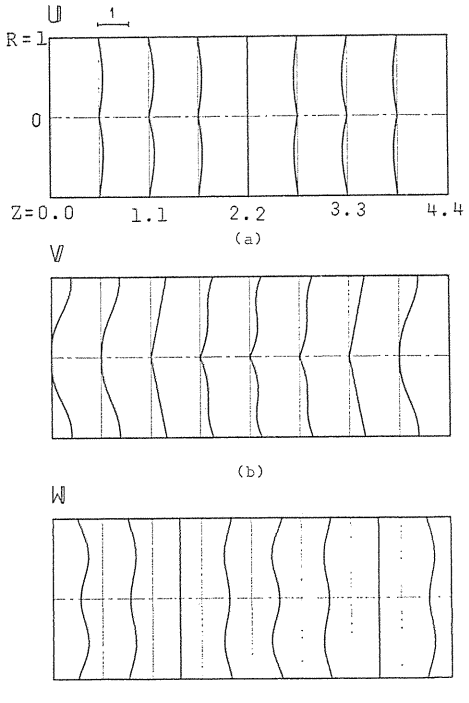

Fig. 2. 10. Velocity component profiles of $s=2$ mode.

successive double helix. The sectioned-streamlines are shown in Fig. 2.9, and the velocity component profiles are shown in Fig. 2.10. From comparison of Fig. 2.7 (c) for $s=1$ and Fig. 2.10 (c) for $s=2$ with Fig. 2.4 (c) for $s=0$, it is seen that the stationary breakdown of the non-axisymmetric type does not exhibit a rapid deceleration or a stagnation. This differs from the case of the axisymmetric type (which agrees with the observation of Leibovich). In addition, the non-axisymmetric type breakdown does not show periodic character in the axial direction. (Although the corresponding sectioned streamlines show periodic variation in the axial direction, the streamlines themselves do not show the periodicity due to the simultaneous variation of the azimuthal velocity.) This also differs from the case of the axisymmetric type.

It has been mentioned that typical modes of the observed stationary breakdown correspond well to the flow field involving the stationary wave of $s=0$, 1 and 2. From this fact, it can be inferred that basic modes of observed breakdowns, including the unsteady case, can be explained as three cases of the flow field perturbed by the wave disturbances with the parameter $s=0$, 1 and 2. From this viewpoint, characteristic flow patterns for these three cases are shown in Fig. 2.11. The figure indicates the streamlines sectioned by the plane $Z=0$ [calculated from $dr/u=rd\theta/v$ c. f., Eq. (2.14)]. As seen from the figure, $s=0$ type shows the axisymmetric flow pattern, $s=1$ type shows the flow deflection in the radial direction and has one axis of symmetry, $s=2$ gives the flow pattern with two axis

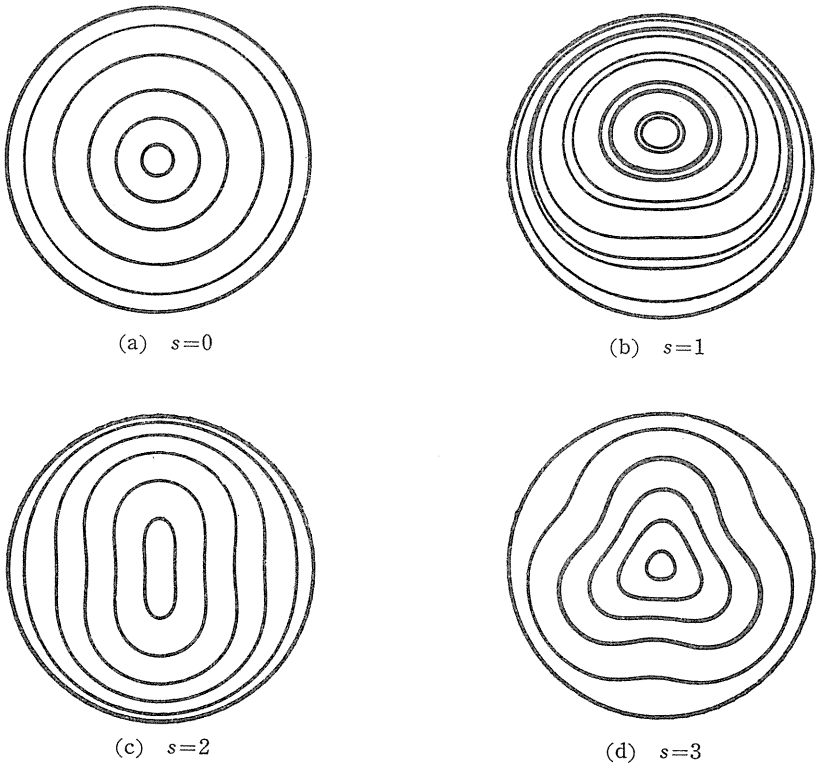

(a) $s=0$ (b) $s=1$

(c) $s=2$ (d) $s=3$

Fig. 2.11. Sectioned-streamlines by $z=0$ plane.

of symmetry. In addition the case of $s=3$ is shown for reference. The breakdown of $s=3$ mode is expected to be a triple helix type, which has not been observed yet.

2. 3. 3. Other Types of Stationary Breakdown

As mentioned before, Leibovich reported on new types of the breakdown, namely, the flattened bubble type 4, and type 3 which exhibits the combined properties of types 2 and 4. Type 4 is explained here (unsteady types 2 and 3 are discussed in next chapter). Leibovich stated that this type is not always stationary, but the inclination of the flattened bubble remains almost constant in the azimuthal direction. This type of breakdown can be explained in terms of the coexistence of $s=0$ and $s=2$ modes of the wave disturbance. Figure 2. 12 shows the calculated streamlines in the case of such coexistence, showing that the streamlines which start from neighbouring positions of the center of pipe section, expand into a flattened bubble inclined in the azimuthal direction. This corresponds well to the observed flow pattern of the type 4 breakdown. The result suggests that various types of breakdown will possibly occur due to the coexistence of two waves with different modes.

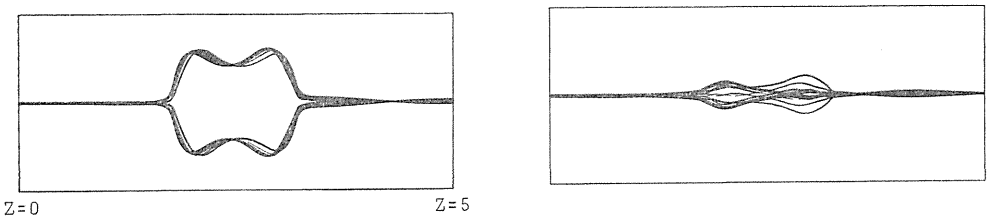

(a) Streamlines viewed from the vertical direction.

(b) Streamlines viewed from the horizontal direction.

Fig. 2. 12. Flow pattern involving two wave disturbances of different modes ($s=0$ and $s=2$).

2. 4. Conclusions

This paper concerns the vortex breakdown phenomena, especially the stationary ones, which occur in a swirling flow within a circular pipe. The shape of the flow fields which involve a neutrally stable wave disturbance is examined. It is made clear that the stationary vortex breakdown has close relation to the occurrence of a wave disturbance without phase velocity. It is also found that various types of breakdown, which have been observed, correspond to the values of a parameter s which defines the azimuthal mode of the wave disturbance.

3. Vortex Breakdown Phenomena of Unsteady Type

3. 1. Introduction

In the preceding chapter, we proposed a qualitative explanation of the vortex breakdown occurring in a pipe. There, it was found that the breakdown phenomena

should depend greatly upon the inertial wave (wave disturbance), the occurrence of which induces an abrupt change in a swirling flow field. It was also pointed out that various types of breakdowns, such as axisymmetric, spiral and double helix types, correspond to the azimuthal modes of the wave disturbances. The preceding chapter, however, treated only steady (or stationary) types of breakdowns. Sarpkaya, Leibovich and many others reported in their experimental studies that among the breakdowns visualized with dye filaments, there are unsteady types in which the streaklines rotate periodically with time on the swirling axis (pipe axis). The present chapter concerns these unsteady types of breakdowns, and shows that these types have a close relation to the phase velocity with which the wave disturbance propagates in the swirling flow in a pipe.

3. 2. Properties of Wave Disturbance

The properties of the wave disturbance represented by Eq. (2.7) are examined in detail here. As seen from Eq. (2.7), when the integer parameter s is assumed to be zero, the disturbances becomes axisymmetric and propagates only in the axial direction (the z direction). On the other hand, $s \neq 0$, the disturbance propagates both in the axial and azimuthal directions. It is also found in the preceding chapter that the parameter s specifies the azimuthal mode of the disturbance so that $s=0$, 1 and 2 correspond to the axisymmetric, spiral and double helix types, respectively.

In the discussion given below, the following nondimensional quantities are used:

$$\left.\begin{aligned} &R_0(\text{Rossby number}) = W_0/(a\Omega), \quad N = n/\Omega, \quad M = am \\ &\sigma' = a\sigma, \quad T = \Omega t, \quad A' = A/(a\Omega), \quad R = r/a, \quad Z = z/a \end{aligned}\right\} \tag{3.1}$$

The angular frequency of disturbance can be derived from Eq. (2.8), that is,

$$N_{\pm} = s + MR_0 \pm 2\sqrt{M^2/(M^2+\sigma'^2)} \tag{3.2}$$

and the axial phase velocity (N/M) is written as

$$N_{\pm}/M = (s/M) + R_0 \pm 2\sqrt{1/(M^2+\sigma'^2)} \tag{3.3}$$

where the double sign in Eqs. (3.2) and (3.3) corresponds to that of Eq. (2.9). The wave disturbance given by Eq. (2.7) indicates a forward or backward progressive wave when the value of N/M is positive or negative, respectively. When $N/M=0$ it becomes a stationary wave which is fixed in the space. As mentioned in the preceding chapter, such a stationary wave disturbance explains a stationary type of observed vortex breakdown.

Figure 3.1 plots the axial phase velocity N/M versus the wave length L_z ($L_z = 2\pi/M$, to be negative for $M<0$) for $s=0$, 1 and 2. In the figure the Rossby number R_o is taken as unity. The corresponding curves for any value of R_o can be obtained by shifting vertically the curves for $R_o=1$, since as seen from Eq. (3.3) intersecting point with the ordinate axis is at $N/M=R_o$, and the value of N/M is proportional to R_o. Figures (a) and (b) give the corresponding curves for the positive and negative signs of the double sign in Eq. (3.3). The intersecting points of the curves and the abscissa ($N=0$) determine the wave length of the stationary wave mentioned above. These figures, calculated from Eqs. (2.9)

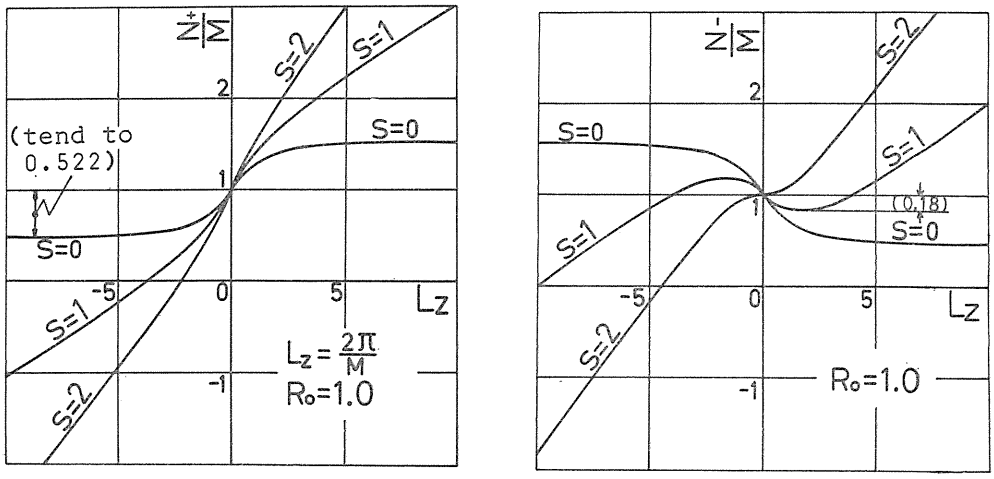

(a) (b)

Fig. 3. 1. Axial phase velocity of disturbance versus wave length.

and (3. 3), represent the following properties of the wave disturbance occurring in a swirling flow; (i) For any value of the parameter s, the axial phase velocity of wave disturbance coincide with the axial velocity of the primary flow in the limit of infinitesimal wave length. (ii) As the axial velocity of the primary flow, W_0, becomes large, the range for the existence of a forward progressive wave becomes large and the absolute wave length of the stationary wave also becomes large. (iii) In the case of $s=0$, for the range of $R_o>0.522$, the phase velocity is always positive so that the disturbance with any wave length is a forward progressive wave. For the range of $R_o<0.522$, there exists such a wave length for the disturbance to be a stationary wave. (iv) In the case of $s=1$ or 2, there are two stationary waves with different wave lengths for any Rossby number. Furthermore, for $s=1$ mode, two more stationary waves can exist when $R_o<0.18$. (v) When $R_o=0$, that is, when the axial velocity of primary flow is absent, all types of disturbance with any wave length are to be unsteady, except a disturbance of $s=1$ with a certain wave length. (vi) Only when $W_0=0$ can there exist a pair of forward and backward progressive waves whose wave length and absolute phase velocity are both equal so that a standing wave, expressed as a sum of them, can take place in a swirling flow. (The term 'standing' is used here for waves which have a node and a loop in the axial direction.)

As mentioned above, the disturbance occurring in a swirling flow exhibits different characteristics depending on the values of parameters R_o, s and M.

3. 3. Unsteady Wave Disturbance and Unsteady Type Vortex Breakdown

The flow patterns of the disturbance given by Eqs. (2. 7) and (2. 10), are here examined, and a close relation between the disturbance and the vortex breakdown is clarified. As mentioned before, the purpose of this study is not to discuss the occurrence mechanism of breakdown or give a precise model including the nonlinear effect, but to explain the various flow patterns of breakdown through qualitative discussions. Therefore we assume that the disturbance is neutrally stable as given by Eq. (2. 7) [however, in fact, Eq. (2. 3) involves solutions other than the neutrally

stable one], and the following figures are calculated by taking the magnitude of the disturbance as the order of unity in spite of the assumption of a small disturbance. In the following, most of the figures plot the calculated streaklines for comparison to the corresponding experimental results visualized with dye.

3. 3. 1. Flow Pattern with Axisymmetric ($s=0$) Disturbance and Breakdown of Bubble Type

Next we examine the unsteady flow perturbed by the disturbance of $s=0$ with a finite phase velocity ($N/M \neq 0$). Figure 3. 2 shows the calculated streaklines for the case of a forward progressive wave of the $s=0$ disturbance ($N/M>0$).

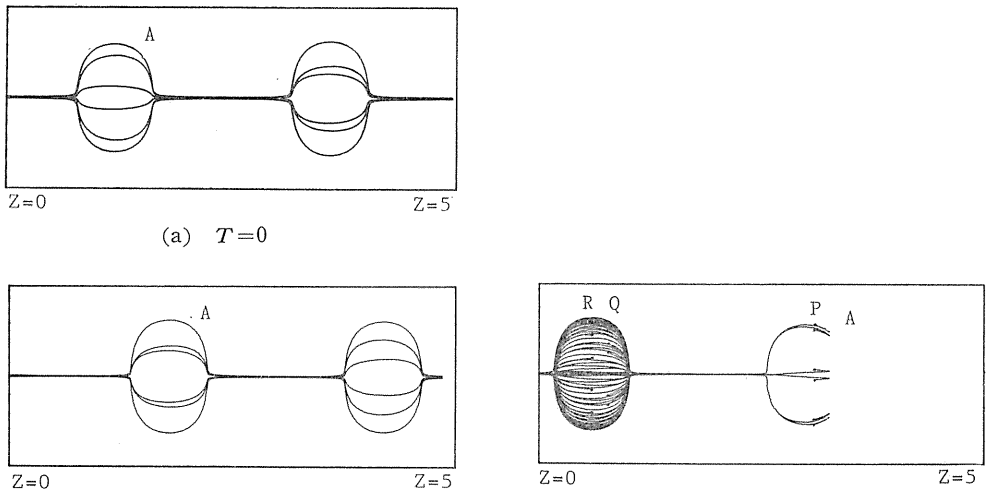

(a) $T=0$

(b) $T=\tau/4$

(c) $T=3\tau/4$

$s=0$, $R_o=0.5$, $N=-0.024$, $M=-2.62$, $A'=1.0$,
$N/M>0$: a forward progressive wave

Fig. 3. 2. Unsteady breakdown of axisymmetric type (streaklines).

The streaklines are calculated by computer, using Eqs. (2. 7) and (2. 10), and the results are obtained as the plotter output. Each figure describes six streaklines which surround the pipe axis with a small circle at the upstream end (here, $Z=0$, and the disturbance is assumed to exist in the region of $Z>0$). Figures (a), (b) and (c) show the streaklines at time $T=0$, $1/4\tau$ and $3/4\tau$, respectively ($\tau=2\pi/|N|$). As seen from these figures, the axisymmetric vortex bubble, with a phase velocity of $|N|/|M|$. It should be noted that Fig. (c) shows discontinuous streaklines. In the experiment of flow visualization with dye, this discontinuity corresponds to the disappearance of the dye filament (which was reported by Sarpkaya[19]). In Fig. (c) discontinuity exists at points P, Q and R (each denoted by six dots). The streaklines, which come from the vicinity of the pipe axis at the upstream end, pass just outside of the first bubble, and after forming a part of the next bubble, they jump back to the inside of the first one (P→Q), circulating several times there to jump again from the position R to an area far downstream ($Z>5$). This means that the fluid particles incide the bubble pass through the upstream end

earlier than the particles just outside the bubble, which may give an interesting suggestion concerning the growth of the bubble.

So far we have treated only the case of a forward progressive wave. It is noted that for the case of a backward progressive wave, the flow pattern is almost same as that of the forward progressive one, except that the bubble moves upstream with time. We now discuss the relation between the theoretical flow pattern mentioned above and the breakdown of bubble type. For a fixed primary flow most of the bubble type breakdowns so far observed are nearly stationary phenomena, although they are often accompanied by small fluctuations. (It has been discussed in the preceding chapter that the stationary breakdown can be explained by the stationary wave of $s=0$ mode which has no phase velocity.) However, Sarpkaya observed in his experiment that the existing vortex bubble moves upstream or downstream along the swirling axis, when the primary flow is accelerated or decelerated by changing rapidly the opening of throttle valve installed at the end of the test tube. Sarpkaya called this a 'travelling vortex breakdown'. Although the result of Fig. 3.2 is derived under the assumption of a fixed primary flow, it explains the moving vortex bubble, and Sarpkaya's travelling vortex breakdown corresponds to the altering streakline with time which is caused by the wave disturbance propagating with a phase velocity. (According to Sarpkaya's experimental results, when the primary flow settles in a new state, the vortex bubble reaches a fixed position, and becomes a stationary breakdown.) In Sarpkaya's experiment the coexistence of two vortex bubbles is observed in the transient of primary flow. These facts also suggest that the occurrence of the progressive wave disturbance is possible in an actual swirling flow, and the corresponding streaklines account for the moving bubble.

3. 3. 2. Flow Pattern with Non-axisymmetric Disturbance ($s=1$, 2)

In this section the relation between the wave disturbance of the $s=1$ mode and the unsteady vortex breakdown of the spiral type is discussed, and then the flow pattern of the unsteady disturbance for $s=2$ is treated briefly.

3. 3. 2. 1. Vortex Breakdown of Spiral Type

Leibovich found a stationary spiral vortex breakdown (his type 6) where dye filament formed a gentle spiral curve. However, typical spiral type of breakdown, which have been reported so far, is such an unsteady phenomenon in which the spiral streakline of dye filament rotates periodically on the swirling axis.

Figure 3.3 gives a result of calculated streaklines of the flow field in which a backward progressive wave of the $s=1$ mode exists. Figure (a) plots the streaklines at time $T=0$, which shows that six streaklines, passing through the vicinity of the axis ($R=0.01$) at the upstream end ($Z=0$), move together into a spiral form. Figure (a)′ is a view of Fig. (a) from downstream side, and Figs. (b) through (e) indicate the successive streaklines at intervals of 1/8 period. The arrow labelled in the figure denotes the rotational direction of primary flow, and the arrows along the streaklines indicate their downstream direction. These figures show that the streaklines rotate on the axis with a period of $\tau=2\pi/N$, and that for this case (the parameter values are given under the figures), the sense of the helix and its rotational direction are the same as that of the swirling primary flow. Figure 3.4 shows a calculated result of a forward progressive wave ($N/M>0$) with $s=1$. Figures (a) and (b) plot the streaklines at times $T=0$ and $3/8\tau$,

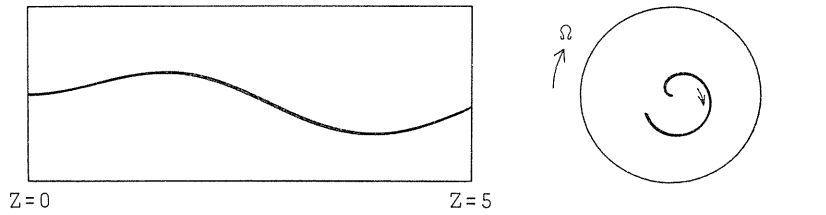

(a) $T=0$ (a)′

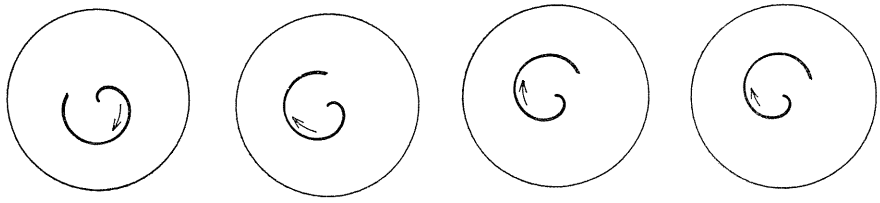

(b) $T=\tau/8$ (c) $T=\tau/4$ (d) $T=3\tau/8$ (e) $T=\tau/2$

$s=1$, $R_o=1.0$, $N=0.0015$, $M=-1.65$, $\sigma'=4.77$, $A'=0.5$,
$N/M<0$: a backward progressive wave

Fig. 3. 3. Streaklines of spiral type breakdown.

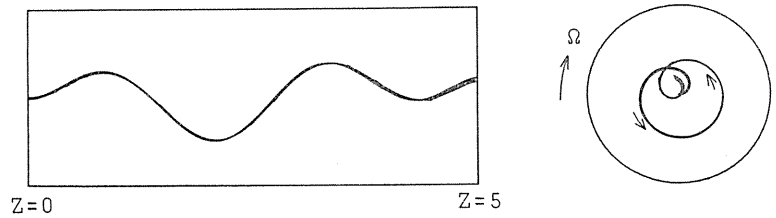

(a) Streaklines at $T=0$.

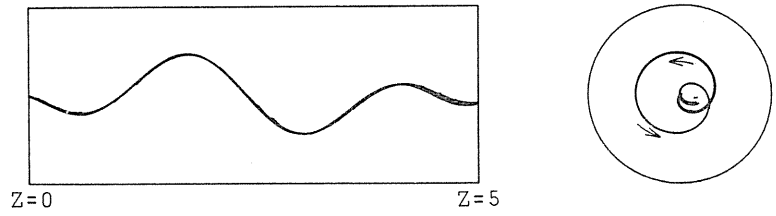

(b) Streaklines at $T=3\tau/8$.

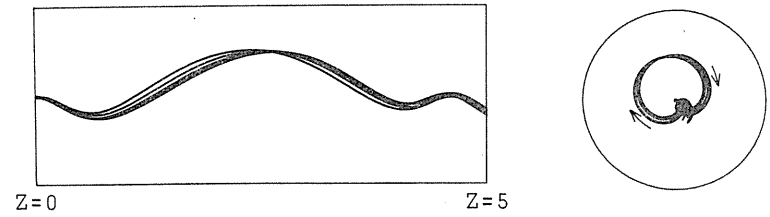

(c) Pathlines for $T=0\sim9.5$.

$s=1$, $R_o=0.4$, $M=1.57$, $N=2.26$, $\sigma'=4.75$, $A'=0.5$

Fig. 3. 4. Spiral type Breakdown for a forward progressive wave.

respectively, and Fig. (c) plots the corresponding pathlines, i. e., the trajectories of fluid particles which depart from the upstream end at $t=0$. For this case the sense of the helical streaklines is in the opposite direction to the primary flow. However, as seen from Fig. (c) the fluid particles themselves move downstream rotating in the same direction as the primary flow. The relation between the sense and the rotational direction is summarized in Table 3. 1, where the sign of the sense and the rotational direction are taken to be positive when they are in the same direction as the primary flow rotation. The sense has an opposite sign to the value of M/s, and the rotational direction has the same sign as the value of N/s. It should be noted that the rotational period of the streaklines is given by $\tau=2\pi s/|N|$.

Table 3. 1. Relation between the characters of streaklines and the parameters of $s=1$ disturbance.

No.	N/s	N/M	M/s	Sence of helix	Direction of rotation
1	+	+	+	(−)	(+)
2	+	−	−	(+)	(+)
3	−	+	−	(+)	(−)
4	0 (Steady flow)	0	−	(+)	Fixed streakline

We now compare the flow pattern mentioned above with the observed vortex breakdown. The breakdown in which the helix form of streakline rotates periodically on the pipe axis, have been reported in detail by Sarpkaya and Leibovich under the labels of spiral type (Sarpkaya) and type 2 (Leibovich). According to their observation of the vortex breakdown phenomena in a pipe, the central streakline of dye filament deflects rapidly at an axial position and forms a helix curve, and the sense of the helix and its rotational direction are the same as the primary flow. These experimental results agree with the flow pattern for the disturbance of a progressive wave mentioned before, and the sense and rotational directions correspond to the case No. 2 of Table 3. 1 (a backward progressive wave). The conclusion is that the spiral type of breakdown reported by Sarpkaya (called type 2 by Leibovich) should be such phenomenon that a progressive wave disturbance of the mode $s=1$ occurs in a actual swirling flow field.

In the experiments, the spiral type vortex breakdown is usually observed in a pattern of sharp twist or abrupt kink, rather than gentle helix, and persists in one or two turns before breaking up into a large-scale turbulence. In order to explain such kinks, the flow pattern with the wave disturbance is further examined. Figure 3. 5 shows the calculated streaklines for a backward progressive disturbance of the $s=1$ mode. According to the order of Figs. (a) to (c), the phase velocity N/M, with which the wave propagates upstream, is evaluated as larger value, while the Rossby number and the amplitude of disturbance are kept constant. When the

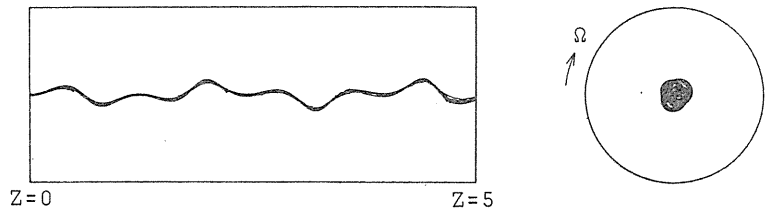

(a) $N/M=-0.041$, $M=-7.85$, $\sigma'=5.10$, $T=0$.

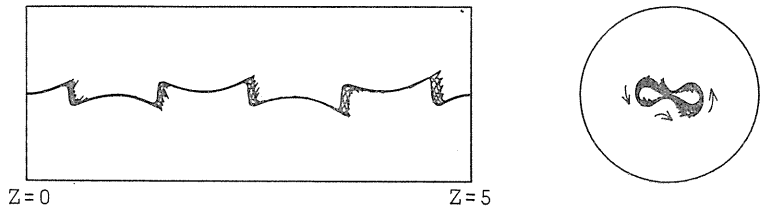

(b) $N/M=-0.36$, $M=-3.14$, $\sigma'=4.97$, $T=0$.

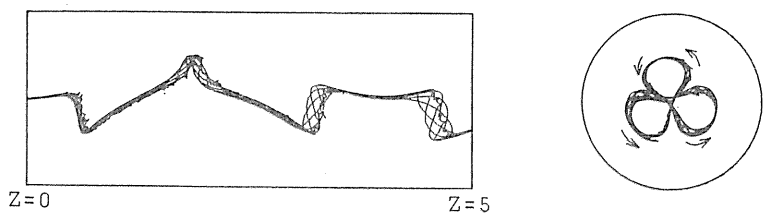

(c) $N/M=-0.91$, $M=-1.25$, $\sigma'=4.66$, $T=0$, $s=1$, $R_0=0.3$, $A'=0.5$.

Fig. 3. 5 Breakdown of kink type.

phase velocity is relatively small compared to the axial velocity of the primary flow, as in Fig. (a), the streaklines form a gentle helix. But when the phase velocity is large, as in Fig. (b) and (c), the streaklines show abrupt kinks. From Fig. 3. 5 and other calculated results for various conditions, it can be said that the kink type breakdown occurs when the $s=1$ mode disturbance propagates with a relatively large velocity. Although Fig. 3. 5 shows periodic kinks, it is considered that only a few kinks can be observed in an actual swirling flow because the flow is largely disturbed behind the kink due to an abrupt change of the flow state. Taking notice of the sense of the helical streaklines, it is found that the sense is opposite to that of primary flow rotation. (It corresponds to the case No. 1 in Table 3. 1.) The vortex breakdown with such character as above was observed by Lambourne[10] in his experiment on the vortex breakdown of the swirling flow on delta wings.

3. 3. 2. 2. Vortex Breakdown of Double Helix Type

Figure 3. 6 plots the calculated streaklines for a forward progressive wave of $s=2$ mode. It describes 12 streaklines which surround the axis with a small circle ($R=0.01$) at the upstream end, expand along the axis into a sheet, both edges of which then twist and form helical lines. This type of breakdown is called double

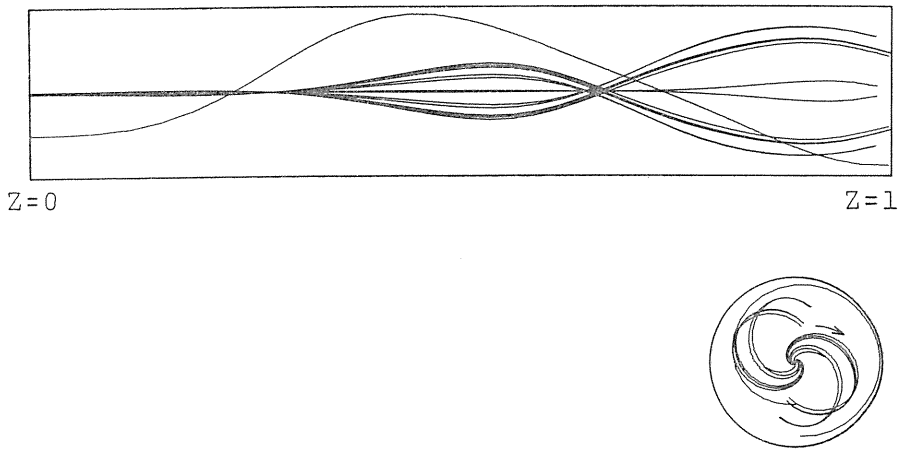

$s=2$, $R_o=1.5$, $M=-1.75$, $N=-0.042$, $A'=1.0$, $\sigma'=5.81$,
$N/M>0$: forward progressive wave

Fig. 3. 6. Breakdown of double helix type.

helix type. (In the figure a streakline which departs from the radial position of $R=0.4$ is also presented.) The double helix type breakdowns, which have been observed so far, is always stationary ones (which correspond to the stationary wave of the $s=2$ mode as mentioned in the preceding chapter). However, for the case of the progressive wave disturbance, the corresponding streaklines rotate on the axis with a period of $\tau=2\pi s/|N|$. The reason why such a mode of breakdown is not observed in experiment is inferred to be that the boundary condition at the inlet of pipe, namely the flow condition at this location, does not fit in usual arrangement of apparatus. From the above cosideration, together with the previous ones on the stationary vortex breakdowns, almost all the types of breakdown that have been reported by Sarpkaya and Leibovich are explained consistently in relation to the wave disturbance which occurs in a swirling flow. It should be noted that the type 3 of Leibovich, which we have not yet discussed (Leibovich has identified six types, type 3 being that the central filament decelerates rapidly and moves abruptly off the axis to form a sharp kink and filament oscillates from side to side in a preferential plane) is considered from the viewpoint of this study to be the flow state in which both the stationary wave of the $s=2$ mode and the progressive wave of the $s=1$ mode exist at the same time.

3. 4. Wave Disturbance in Actual Swirling Flow and Breakdown

So far, as to the primary flow, we have assumed that it is rigidly rotational with uniform axial velocity. In the following we apply the experimental formula given by Leibovich[20] to the velocity profile of primary flow, and we will point out that an approach similar to that mentioned above is also valid in explaining the vortex breakdown in an actual swirling flow.

Leibovich measured the velocity profile of primary flow of a swirling flow field where the breakdown phenomenon took place, and introduced the following experimental formula.

$$\left.\begin{aligned}\bar{V}(R) &= \frac{K}{R}(1-e^{-qR^2}) \\ W(R) &= W_1 + W_2 e^{-qR^2}\end{aligned}\right\} \tag{3.4}$$

where K, q, W_1 and W_2 are positive constants.

Next, we will describe a method to derive the wave disturbance when the $\bar{V}(R)$ and $\bar{W}(R)$ of the primary flow are functions of R. The differential equations which govern the disturbances $\tilde{u}$, $\tilde{v}$, $\tilde{w}$, and $\tilde{p}$, are linear with real coefficients as stated in Chapter 2 (the equations can be introduced from the Euler equation and the continuity equation). Hence, a complex solution is first obtained and then a real solution can be derived as the sum of the conjugate pair. Now, the disturbance components $\tilde{u}$, $\tilde{v}$, $\tilde{w}$ and $\tilde{p}$ are put in the following form:

$$\left.\begin{aligned}\tilde{u} &= U(r)\, e^{-i(s\theta+mz)+\lambda t} \\ \tilde{v} &= V(r)\, e^{-i(s\theta+mz)+\lambda t} \\ \tilde{w} &= W(r)\, e^{-i(s\theta+mz)+\lambda t} \\ \tilde{p} &= P(r)\, e^{-i(s\theta+mz)+\lambda t}\end{aligned}\right\} \tag{3.5}$$

where $U(r)$, $V(r)$, $W(r)$ and $P(r)$ are complex functions of r, and λ is a complex number. Substituting Eq. (3.5) into the governing equations of disturbances mentioned above, the following equation with respect to only $U(r)$, after the elimination of V, W and P.

$$\begin{aligned}&\frac{d^2U}{dr^2}+\frac{3s^2+r^2m^2}{s^2+r^2m^2}\frac{1}{r}\frac{dU}{dr}-U\frac{1}{r^2}\left\{\frac{r^2m^2-s^2}{s^2+r^2m^2}+r^2m^2+s^2\right\} \\ &=\frac{1}{\lambda-is(\bar{V}/r)-im\bar{W}}\frac{(-is)}{r^2}\left\{\left(r\frac{d^2\bar{V}}{dr^2}+\frac{d\bar{V}}{dr}-\frac{\bar{V}}{r}\right)\right. \\ &\left.-\frac{2r^2m^2}{s^2+r^2m^2}\left(\frac{d\bar{V}}{dr}+\frac{\bar{V}}{r}-\frac{s}{rm}\frac{d\bar{W}}{dr}\right)-\frac{r^2m}{s}\left(\frac{1}{r}\frac{d\bar{W}}{dr}-\frac{d^2\bar{W}}{dr^2}\right)\right\}U \\ &+\frac{1}{\{\lambda-is(\bar{V}/r)-im\bar{W}\}^2}\frac{\bar{V}}{r}\left(\frac{d\bar{V}}{dr}+\frac{\bar{V}}{r}-\frac{s}{rm}\frac{d\bar{W}}{dr}\right)2m^2U\end{aligned} \tag{3.6}$$

The boundary condition of pipe wall [i. e., $U(r)=0$ at $r=a$] specifies the eigenvalue and the eigenfunction $U(r)$. Since it is difficult to solve the above equation analytically, we instead use a computer to obtain the numerical solutions of and $U(r)$.

In the first place, we describe a calculated result for the axisymmetric vortex breakdown ($s=0$ mode). Figure 3.7 plots the velocity profile of the primary flow given by Eqs. (3.4). Figure 3.8 describes some calculated streaklines for the axisymmetric stationary wave ($s=0$, $\lambda=0$) which exists in a flow field shown in Fig. 3.7. In this case the flow is steady so that the streaklines coincide with streamlines or pathlines. The flow pattern as shown in Fig. 3.8 agrees with the stationary bubble type breakdown. This result indicates that a wave disturbance without phase velocity and of $s=0$ mode corresponds to the stationary bubble type

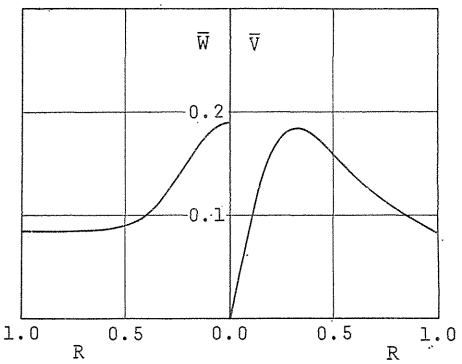

$W_1=0.086$, $W_2=0.104$, $q=11.84$, $K=1/11.84$

Fig. 3. 7. Velocity profile of primary flow represented by Eq. (3. 4).

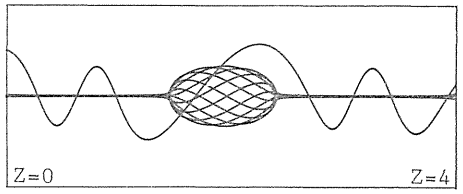

$s=0$, $R_o=0.19$, $\lambda=0.0$, $M=-2.0$

Fig. 3. 8. A calculated result of axisymmetric breakdown for the primary flow given in Fig. 3. 7.

Table 3. 2. Angular frequency $N$and phase velocity N/M for both cases of rigidly rotational flow with uniform axial velocity and primary flow given by Eq. (3. 4).

$M(2\pi/M)$		3(2. 09)	1(6. 28)	−1(−6. 28)	−3(−2. 09)	−6(−1. 05)	−12(−0. 50)
(1)	N	1. 80	0. 69	0. 32	0. 68	0. 55	−0. 36
	N/M	0. 60	0. 69	−0. 32	−0. 22	−0. 092	0. 030
		+	+	−	−	−	+
(2)	N	0·97	0. 34	0. 014	0. 0*	−0. 15	−0. 71
	N/M	0. 32	0. 34	−0. 014	0. 0	0. 024	0. 059
		+	+	−	0	+	+

(1) rigidly rotational flow with uniform axial velocity
(2) primary flow given by Eq. (3. 4) (same parameters as Fig. 3. 8)
$R_o=0.19$ (defined by the values at the vicinity of pipe axis)
+: forward progressive wave, −: backward progressive wave, 0: stationary wave

breakdown, even in the case of actual flow field. In addition, although Fig. 3. 8 shows a steady flow due to the stationary wave, the progressive wave can also exist for the experimentally obtained primary flow. Table 3. 2 indicates the angular frequency N and the axial phase velocity N/M of the wave disturbance ($s=0$ mode) with the Rossby number $R=0.19$ for the analytical and the actual primary flows. As seen from the table, the wave disturbance can be a forward or backward progressive wave or a stationary wave, depending on the values of the axial wave number M (or wave length $2\pi/M$), which agrees qualitatively with the result of Fig. 3. 1 based on anaxially uniform and rigidly rotational primary flow. Figure 3. 8 corresponds to the result for the disturbance (stationary wave) denoted by * in Table 3. 2. If $M=-6$ is chosen, for example, the disturbance has a positive

phase velocity, and the corresponding streaklines represent a moving bubble in the same manner as Fig. 3.2. The effect of the velocity profile of the cylindrical primary flow appears in the eigenfunctions of $U(R)$, $V(R)$, $W(R)$ and $P(R)$. A comparison is given in Fig. 3.9 for the eigenfunction $U(R)$ in both cases of the analytical solution [$U(R)=kJ_1(\sigma' R)$; k: a constant] for rigidly rotational flow with uniform axial velocity and the numerical one for an actual swirling flow. The analytical eigenfunction $U(R)$ does not depend on the values of the Rossby number R_o and the wave number M so that $U(R)=kJ_1(\sigma' R)$ always holds. However, the eigenfunction $U(R)$ for an actual swirling flow depends on the values of R_o and M, though it takes a similar form qualitatively. The difference of $U(R)$ from the analytical one becomes large at a position far off axis, and small in the vicinity of axis. From the fact that in the vortex breakdown a drastic change occurs near the pipe axis, it can be said that the results from the analytical solution do explain qualitatively the breakdown phenomenon occurring in an actual swirling flow. Furthermore, it is confirmed that Eq. (3.6) involves the solutions of the wave disturbances ($s\neq 0$) of non-axisymmetric types.

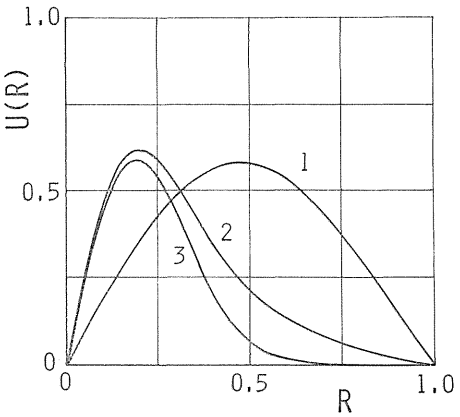

1: rigidly rotationary flow with uniform axial velocity [$J_1(\sigma' R)$], 2, 3: primary flow given by Eq. (3.4) (2: $M=-3$, 3: $M=-12$)

Fig. 3.9. Comparison of eigenfunction $U(R)$.

3.5. Conclusions

In this chapter, assuming the primary flow to be rigidly rotational with uniform axial velocity, it is found that the occurrence of a progressive wave disturbance corresponds well to the flow pattern of the observed unsteady breakdown in a swirling flow. It is also found that the analytical results concerning the flow pattern of breakdown can be applied to an actual swirling flow field.

4. Experiments on Flow Patterns of Vortex Breakdown

4.1. Introduction

Vortex breakdown phenomena occur in various forms and present complicated flow fields. In the preceding chapters, the authors gave a theoretical explantation on the phenomena, from the viewpoint that they have a close relation with the inertial wave (wave disturbance). It was also pointed out that 3 representative types of breakdown among various flow patterns observed so far, (i) axisymmetric (bubble), (ii) spiral and (iii) double helix types, correspond to the azimuthal wavenumber 0, 1 and 2 of the wave disturbance respectively, and that the timedependence of breakdown phenomena corresponds to the axial phase velocity of the wave

disturbance. In addition, it was proposed that various types other than the above three can be explained in terms of the coexistence of the wave disturbances with different azimuthal wave numbers.

The purpose of this study is to verify the above theoretical predictions by experiments. The discussions are largely limited to the flow patterns of vortex breakdown, and are not concerned with the growing mechanism of wave disturbances.

4. 2. Experiments

Sarpkaya[19] examined the vortex breakdown phenomena in a swirling flow with a slightly divergent pipe, and reported the three types of breakdown mentioned above. Leibovich[20] noted six different types of breakdown, using apparatus similar to Sarpkaya's. In the present study the breakdowns of the swirling flow in a straight circular pipe are examined and visualized with dye filaments of fluorescein sodium solution.

4. 2. 1. Experimental Apparatus

A schematic view of the experimental apparatus is shown in Fig. 4. 1. Water pressurized by a pump is supplied to the upper constant head tank A. Passing

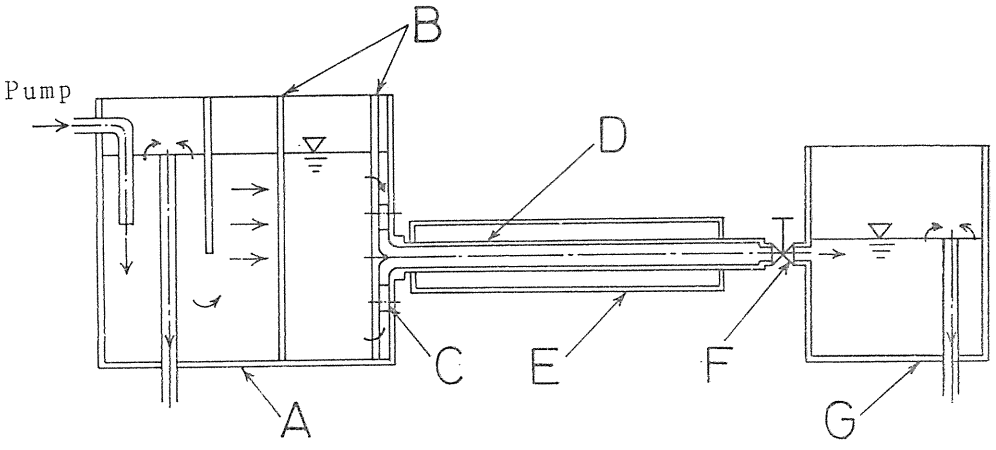

Fig. 4. 1. Experimental apparatus.

through the two honeycombs B, water enters the guide vanes C to get the azimuthal velocity. Then it enters the test pipe D (60 mm inside diameter, 1000 mm in length, made of acryl). The test pipe is covered with rectangular box E (which is filled with water) made of transparent acryl in order to remove the lens effect of the circular pipe at the flow visualization. Through the flow control valve F installed at the downstream end, it enters the tank G and is drained.

Figure 4. 2 shows details of the guide vane and the upstream region of the test pipe. The guide vane has 24 vanes and the angle ϕ is adjustable in the range from 0 to 50°. A and B in Fig. 4. 2 denote capillary tubes (inner diameter 0. 4 mm) for dye injection. Tube A is positioned on the axis of the pipe, and B is movable in the radial direction. In the experiment two dye filaments can be observed at the

same time.

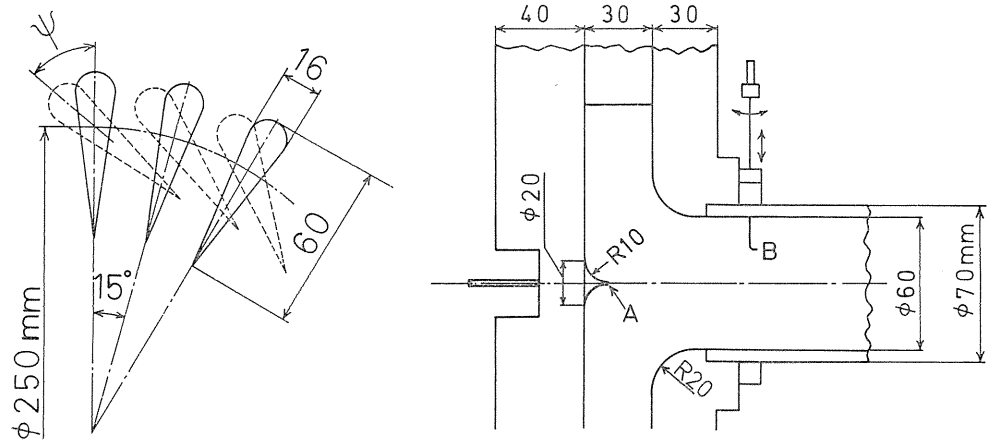

Fig. 4. 2. Guide vane and dimensions of entrance part of pipe.

4. 2. 2. Experimental Method

Various types of breakdown are observed when the flow rate is gradually changed by the valve F with the angle of the vanes kept constant (ψ=30, 35, 40° etc.). The flow fields are recorded by photographs of the dye filaments, and in the case of the unsteady types of breakdown they are photographed by a motor-driven camera.

One of the purposes of this experiment is to realize new types of breakdown, which have not been observed yet but are predicted by the theory proposed in the

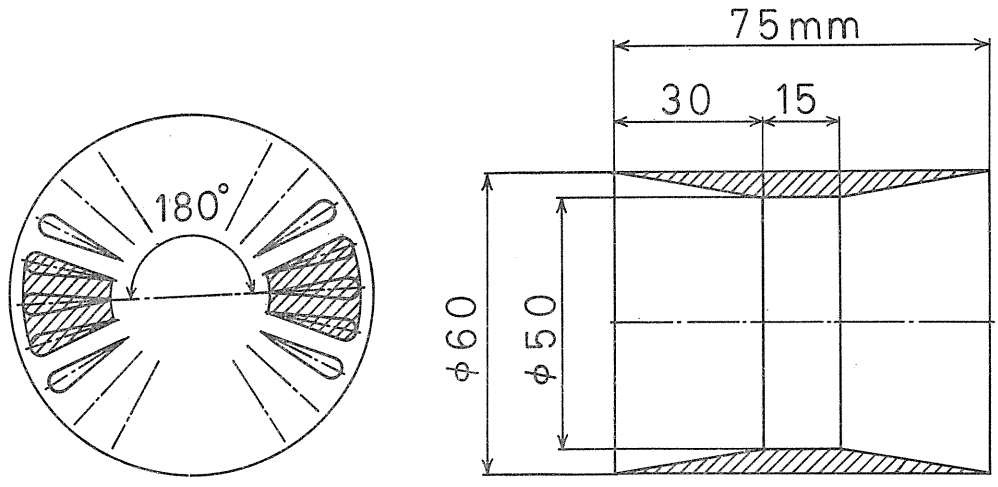

(a) (b)

Fig. 4. 3. (a) Closed parts of guide vane.
(b) Throat inserted into pipe.

preceding chapters. For this purpose it is necessary to change the flow field in a delicate manner. As shown in Fig. 4.3 (a), a part of the guide vane is sometimes blocked during the experiment, or a thin throat shown in Fig. 4.3 (b) is sometimes inserted at a certain axial position of the pipe. The experimental results obtained in above mentioned manner are noted by, for example, "condition of Fig. 4. 3(a)".

4. 3. Comparison of Flow Patterns Based on Theoretical Model with Experimental Results of Breakdown

In the following the photographs of the visualized streaklines of dye filaments are compared with the calculated streaklines which are derived from Eqs. (2.7) and (2.10) as the plotter output of computer. The conditions under which the experiment is carried out or those corresponding to the theoretical calculation are presented under each figure. The following experimental conditions are given: the angle ϕ of guide vane and Reynolds number ($R_e=U_0D/\nu$; U_0: mean axial velocity in the pipe; D: diameter of the pipe; ν: kinematic viscosity). The theoretical conditions are: Rossby number R_o, azimuthal wave number s, axial wave number M, angular velocity N and amplitude A' of the disturbance [c. f. Expression (3.1)].

In the existing circumstances, however, it is difficult to specify the values of the wave number M and the amplitude A' of the disturbance which actually occurs for a actual primary flow. Therefore, in calculating the streaklines from the theoretical model, we choose a suitable wave number and amplitude, and the characteristics of the flow field are compared qualitatively with the experimental results.

In each of the following figures calculated streaklines are shown, the 12 streaklines which surround the pipe axis at the upstream end with the radius $R=0.01$, and a streakline off axis by $R=0.4$ at the upstream end.

4. 3. 1. Elementary Types of Breakdown

As mentioned before, Sarpkaya pointed out that the typical vortex breakdowns are those of axisymmetric type (bubble type), spiral type and double helix type. The elementary type of breakdown, here, means the one which can be explanied by a single disturbance whether the phenomenon is stationary or unsteady.

4. 3. 1. 1. Breakdown of Axisymmetric Type ($s=0$, Bubble Type)

The axisymmetric type breakdown appears in the form of an axisymmetric bubble at a certain axial position of the swirling flow. When the flow field in the pipe is steady, the bubble itself is observed almost stationary in general. However, many researchers reported that the bubble is usually accompanied by another break down of spiral type, which rotates periodically on the pipe axis in the wake region (see Fig. 4.9). The authors observed only a purely stationary breakdown of bubble type, giving a subtle change to the primary flow by blocking a part of guide vane as shown in Fig. 4.3(a). The photograph is given in Fig. 4.4 (a). Although the size is small, the second bubble is observed in the downstream region of the first bubble. Figure 4.4 (b) shows the calculated streaklines which correspond to the stationary wave of $s=0$ type [using Eqs. (2.7) and (2.10) with $s=0$ and $N=0$). For this case, as noted under the figure, the amplitude A' of the disturbance is assumed to decrease to the downstream direction (to compare with the observed one, taking viscocity of real fluid into account). The subscript of each parameter (A', M, N) under the figure denotes the value of s. Both figures

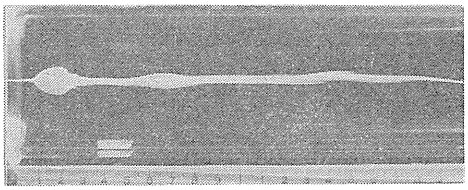

(a) R_e=595, ψ=35°, "condition of Fig. 4. 3 (a)".

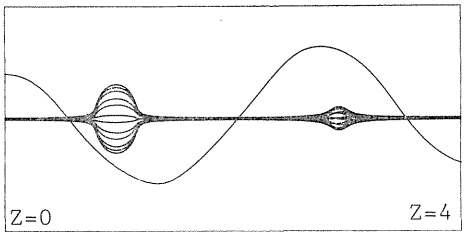

(b) R_o=0.4, s=0, M_0=3.21, N_0=0, A_0'=0.48($Z \leqq 2$), 0.4($Z>2$).

Fig. 4. 4. Breakdown of axisymmetric type (s=0).

4.4 (a) and (b) justify the result from the theoretical model that the occurrence of s=0 mode of disturbance corresponds to the flow pattern of the breakdown of bubble type.

4. 3. 1. 2. Breakdown of Non-axisymmetric Type (s=1 and s=2)

Figures 4.5 and 4.6 show comparisons between observed and calculated breakdowns with respect to the stationary spiral type (s=1) and the stationary double helix type (s=2), respectively. For both cases the flow is steady since the streaklines remain fixed in the space. And the sense of spiral or helix of the streaklines

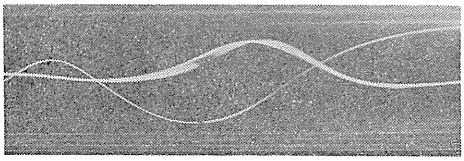

(a) R_e=686, ψ=35°.

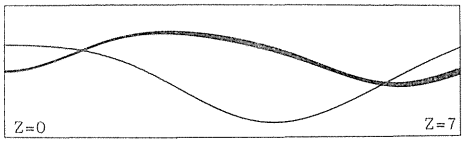

(b) R_o=1.3, s=1, M_1=−1.14, N_1=0, A_1'=1.0

Fig. 4. 5. Stationary breakdown of spiral type.

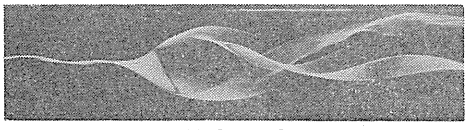

(a) R_e=1158, ψ=35°.

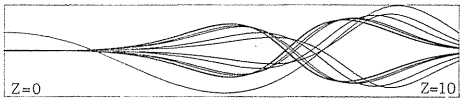

(b) R_o=1.5, s=2, M_2=−1.04, N_2=0, A_2'=1.0.

Fig. 4. 6. Stationary breakdown of double helix type.

is the same with the direction of rotation of the primary flow. This relation holds for s=1 and 2 types of the stationary wave (N=0), as mentioned in the previous chapter. These results confirms that the occurrences of the s=1 and 2 modes of disturbance correspond to the spiral and the double helix types of breakdown, respectively.

In the above, all types of breakdown are stationary ones. However, several observations of the unsteady breakdowns have been reported in which the streak-

line of dye filament leaving upstream near the axis rotates periodically on the axis. There the streakline is fairly different from the one of Fig. 4.5, and shows sharp kinks (Sarpkaya and Leibovich refer to them as the spiral type or kink type). This type of breakdown is also observed in the present experiment. One of the results is shown in Fig. 4.7 (a). Figure 4.7 (b) shows the calculated streaklines for the occurrence of $s=1$ mode of disturbance in which the axial phase velocity is negative and considerably large in absolute value. The calculated ones represent the flow pattern of kink type and the streaklines rotate periodically on the axis. Thus, the breakdown of kink type is also explained from the model of wave disturbance, as pointed out in the preceding chapter. This type is again discussed in the next section.

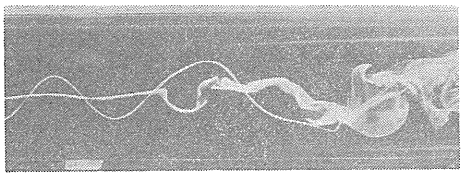

(a) $R_e=1148$, $\psi=35°$.

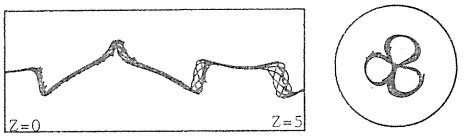

(b) $R_o=0.3$, $s=1$, $M_1=-1.25$, $N_1=1.14$, $A_1'=0.5$
(right figure is a view of streaklines from downstream side).

Fig. 4.7. Breakdown of kink type (unsteady spiral type).

On the other hand, the theoretical model predicts the possibility of the occurrence of a breakdown in which the streakline displays a gentle spiral (not sharp kink) and rotates periodically. It has not yet been reported that only such type of breakdown is observed, although the streaklines in the wake of the bubble of the axisymmetric breakdown are often observed in that form. By experiments we examie whether the above type of breakdown is realized alone. Figure 4.8 (a) shows an example of the gentle spiral type of breakdown which is observd when an ellipsoid made of acryl (major axis, 30 mm; minor axis, 25 mm) is inserted along the axis into the flow field. The corresponding calculated streaklines are shown in Fig. 4.8 (b).

In this section, among various types of breakdown observed in the swirling pipe-flow, types of breakdown are discussed in which the flow patterns can be explained by the occurrence of a single wave disturbance. It is noted that although

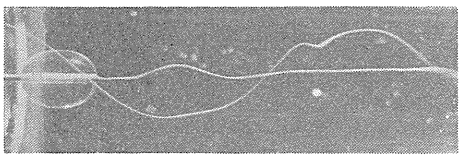

(a) $R_e=950$, $\psi=35°$.

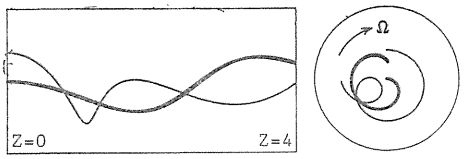

(b) $R_o=0.4$, $s=1$, $M_0=-0.5$, $N_1=0.50$, $A_1'=0.2$
(arrow indicates rotational direction of primary flow).

Fig. 4.8. Breakdown of unsteady gentle spiral type.

the theoretical model gives also the possibility of the occurrence of unsteady axisymmetric type (travelling bubble) or unsteady double helix (double helical streaklines with periodic rotation), such breakdowns were not observed in this experiments (they have not yet been reported by other researchers).

4. 3. 2. Flow patterns of Breakdown with Several Coexisting Modes of Wave Disturbance

There is the possibility, judging from the model, that several wave disturbances with different s values may occur at the same time. The types of breakdown observed in the experiments are demonstrated in the following.

4. 3. 2. 1. Breakdowns Explained by Coexistence of Disturbances of $s=0$ and $s=1$ Modes

Figure 4. 9 (a) shows a photograph of the vortex breakdown which has been so far observed most frequently. The streakline leaving upstream near the axis,

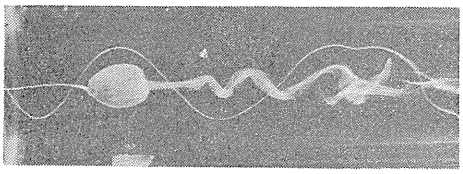

(a) $R_e=1468$, $\psi=35°$.

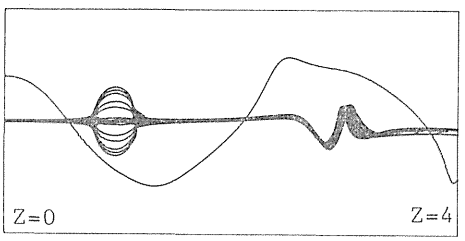

(b) $R_o=0.4$, $s=0.1$, $M_0=3.21$, $N_0=0$, $A_0'=0.48(Z<2)$, $A_0'=0.36(Z\leqq 2)$, $M_1=1.0$, $N_1=1.83$, $A_1'=0\sim 0.1(1\leqq Z\leqq 2)$, $A_1'=0.1(Z>2)$.

Fig. 4. 9. Axisymmetric type breakdown and unsteady spiral type in the downstream region.

forms a bubble at a certain axial position Z, and the downstream end of the bubble somewhat fluctuates. Then the streakline, a part of which reverses into the bubble, stretches together almost in a line along the axis, and at a certain downstream position forms an unsteady spiral type of breakdown which rotates periodically on the axis. For all the similar type breakdowns observed in the experiments, the direction of rotation of the spiral curves was the same as that of the primary flow, but the sense of the spiral was in the opposite direction.

Figure 4. 9 (b) shows the calculated streaklines which explain the above type of breakdown, assuming that a wave disturbance of steady $s=0$ mode (stationary wave) and an unsteady disturbance of $s=1$ mode coexist in the flow field. That is, the axisymmetric disturbance is assumed to exist in the whole field under the same condition as Fig. 4. 4 (b), and the spiral disturbance ($s=1$ type) occurs from the axial position $Z=1.0$ near the downstream end of the first bubble [see Fig. 4. 4 (b)]. Also, the amplitude A' of disturbance of $s=1$ mode is assumed to increase gradually ($Z=1.0\sim 2.0$) and then keep constant ($Z>2.0$). Both figures 4. 9 (a) and (b) show good agreements with respect to the behaviour of streaklines in the downstream of the bubble, namely, the rotational direction and the sense of

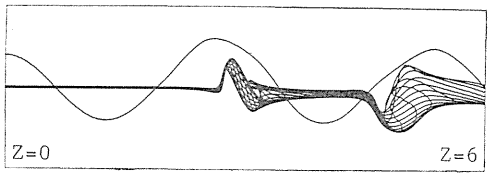

$R_o=0.4$, $s=0.1$, $M_0=3.21$, $N_0=0$,
$A_0'=0.5(Z\geqq 2)$, $M_1=-1.5$, $N_1=1.0$,
$A_1'=0.1(Z\geqq 2)$

Fig. 4. 10. Breakdown regarded as the coexistence of $s=0$ and $s=1$ types.

the spiral breakdown. Next, the kink type of breakdown described in the previous section is discussed again. It can be conjectured that the occurrence of the disturbance of $s=0$ type deforms greatly the streaklines of coexisting wave disturbances. Figure 4. 10 shows the streaklines which are calculated under the condition that the wave disturbance of $s=1$ mode with a negative phase velocity coexists with the $s=0$ mode disturbance from a certain axial position. The breakdown of kink type appears near the upstream stagnation point of the hidden bubble due to the $s=0$ mode wave disturbance. The flow pattern agrees well with Fig. 4. 7 (a). Therefore the breakdown of kink type observed so far is considered possibly as a flow field in which the $s=0$ and $s=1$ mode wave disturbances coexist (however, we do not abandon yet an explanation mentioned in the section 4. 3. 1. 2.).

Other two types of breakdown which have not been reported are shown in Figs. 4. 11 and 4. 12. They are considered as the coexistence of steady axisymmetric type and steady spiral type disturbances, but they appear in different forms for reason that the existing regions of each disturbance are different. In the calculations of both streaklines, the stationary wave disturbance of $s=0$ mode is asummed

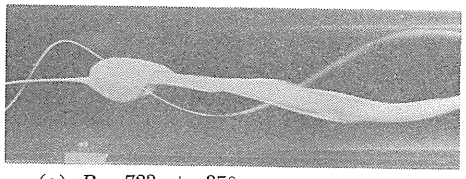

(a) $R_e=723$, $\psi=35°$
"condition of Fig. 4. 3(a)".

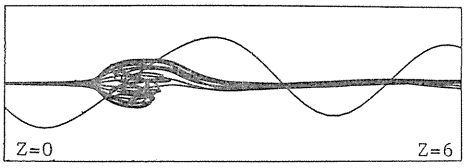

(b) $R_o=0.5$, $s=0.1$, $M_0=1.15$, $N_0=0$,
$A_0'=0.6$, $M_1=-4.74$, $N_1=0$,
$A_1'=0.05(Z\geqq 2.7)$.

Fig. 4. 11. Breakdown arising from the coexistence of stationary wave disturbance of axisymmetric and spiral types.

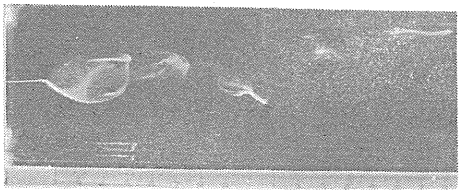

(a) $R_e=989$, $\psi=35°$,
"condition of Fig. 4. 3(a)".

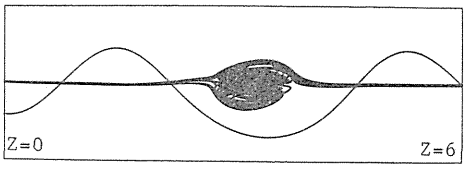

(b) $R_o=0.5$, $s=0.1$, $M_0=1.15$, $N_0=0$,
$A_0'=0.6$, $M_1=-4.74$, $N_1=0$,
$A_1'=0.04(Z>1)$.

Fig. 4. 12. Breakdown arising from the coexistence of stationary wave disturbances of axisymmetric and spiral types.

to exist in the whole region with a constant amplitude (the bubble corresponding to this disturbance locates in the region of $Z=2.1\sim3.4$). On the other hand the region of the stationary wave of $s=1$ mode is that of $Z<2.8$ for Fig. 4.11 and $Z>1.0$ for Fig. 4.12 respectively. For both cases of Fig. 4.11 and 4.12 the theoretical and experimental results agree well with respect to the flow patterns. It is confirmed that some types of breakdown in actual flow field can be attributed to the coexisting wave disturbances of $s=0$ and $s=1$ modes.

4. 3. 2. 2. Breakdowns in Which s=0 and s=2 Types or s=1 and s=2 Types Coexist

Figures 4.13 and 4.14 give two examples of breakdowns regarded as the coexistence of wave disturbances of $s=0$ and $s=2$ modes (both are stationay waves). Figure 4.13 (a) shows a photograph of the breakdown observed when the throat shown in Fig. 4.3 (b) was inserted into the pipe. Two tails, which are fixed in

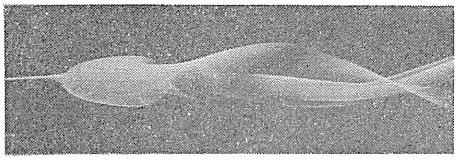

(a) $R_e=704$, $\psi=40°$, "condition of Fig. 4. 3(b)".

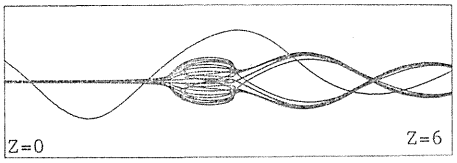

(b) $R_0=0.5$, $s=0.2$, $M_0=1.15$. $N_0=0$, $A_0'=0.6$, $M_2=-2.18$, $N_2=0$, $A_2'=0.2(Z>3)$.

Fig. 4. 13. Breakdown arising from the coexistence of stationary wave disturbances of axisymmetric and double helix types.

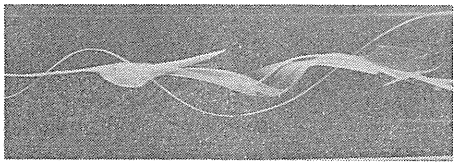

(a) $R_e=878$, $\psi=35°$.

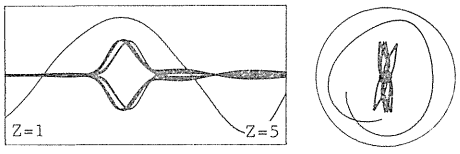

(b) $R_0=0.5$, $s=0.2$, $M_0=1.15$, $N_0=0$, $A_0'=0.5$, $M_2=-6.97$, $N_2=0$, $A_2'=0.5(Z>0)$.

Fig. 4. 14. Breakdowns arising from the coexistence of stationary wave disturbances of axisymmetric and double helix types (flat bubble).

the space, appear from the downstream half of the axisymmetric bubble. Figure (b) shows the streaklines calculated under the condi tion that in addition to the disturbance of $s=0$ mode, the stationary wave of $s=2$ exists in the region of $Z>3.0$. The streaklines in Fig. (b) agrees with those of Fig. (a). Further, Fig. 4.14 is the case in which the stationary wave of $s=2$ exists in a more upstream region ($Z>0$) than in Fig. 4.13. For this case the calculated streaklines appear in the form of a stationary flat bubble (referred to as "type 6" by Leibovich). Figure (c) shows the streaklines viewed from downstream, and figure (a) is a photograph

obtained by experiment.

A flow pattern of breakdown in which two tails from the rear part of the bubble rotate periodically on the axis is shown in the photographs of Fig. 4. 15 (a) and (b). Figure (b) is at the time when the dye filaments rotate by 90° from the state of Fig. (a). In this case the throat was inserted in the upstream region. Figure (c) shows the calculated streaklines, assuming that the stationary wave of $s=0$ and a unsteady wave disturbance ($N/M \neq 0$) of $s=2$ type coexist in the region of $Z>2.9$. The streaklines of Fig. (c) rotate in the same direction of primary flow with a period of $2\pi s/|N|$.

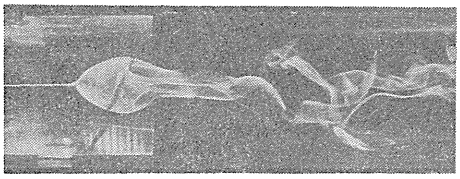

(a) $R_e=1314$, $\psi=35°$
"condition of Fig. 4. 3 (b)".

(b) Flow pattern rotating by the angle 90° from that of Fig. (a).

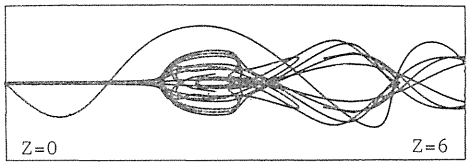

(c) $R_o=0.5$, $s=0.2$, $M_0=1.15$, $N_0=0$, $A_0'=0.7$, $M_2=-1.7$, $N_2=0.43$, $A_2'=0.3$($Z>2.9$).

Fig. 4. 15. Breakdown arising from the coexistence of stationary axisymmetric and unsteady double helix types.

The last example shown in Fig. 4. 16 is the one in which the stationary wave disturbances of $s=1$ and $s=2$ modes are considered to coexist. In this type of breakdown, the streaklines near the axis spread into a sheet at a certain axial position and also form spiral curves fixed in space. (Similar ones have been observed by Leibovich.). Figure (b) shows the calculated one, assuming that the stationary waves of $s=0$ and $s=2$ modes coexist in the region of $Z>0$, and shows good agreement with Fig. (a).

It is concluded that various types of breakdown which have been reported so

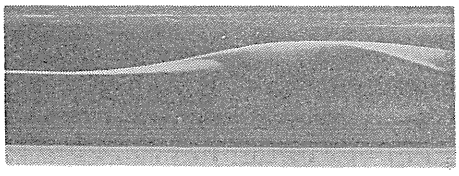

(a) $R_e=468$, $\psi=35°$.

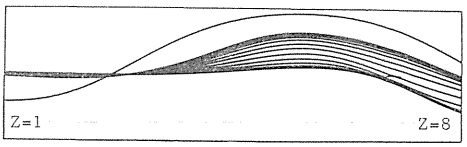

(b)

Fig. 4. 16. Brakdown arising from the coexistence of stationary wave disturbances of spiral and double helix types.

far are classified essentially into three elementary types which correspond to the occurrence of the single disturbance of either mode $s=0$, $s=1$ or $s=2$, and that types other than the above three correspond to the coexistence of the multiple disturbances. It is also found that the range of the coexistence region and the amplitude of the disturbances result in considerable difference in the corresponding flow patterns. It is noted that the flow patterns of all types of breakdown observed to date can be explained by the presented theoretical model of the wave disturbance.

4. 4. *Velocity Profile of Primary Flow and Form of Breakdown*

The calculated streaklines presented so far are based on Eqs. (2.7), which are introduced under the assumption that the primary flow is rigidly rotational with uniform axial velocity. In the following, another example is shown for the case in which the velocity $\overline{V}(r)$ and $\overline{W}(r)$ of primary flow are similar to the actual swirling pipe-flow. The form of the primary flow is assumed to be Leibovich's formula Eq. (3.4). For this case it is impossible to obtain the expressions of wave disturbances in analytical form, as mentioned in section 3.4. The eigenvalue λ and eigenfunctions $U(r)$ etc. in Expressions (3.5) must be numerically solved from Eq. (3.6) as a boundary-value problem. As an example, Fig. 4.17 shows the calculated streaklines for the flow field with the stationary wave disturbance of $s=2$

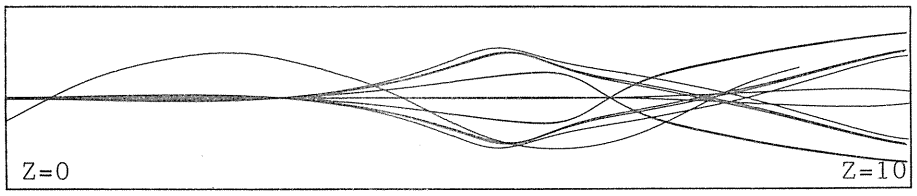

$q=11.84$, $K=(1/11.84)$, $W_1=0.36$, $W_2=0.43$, $R_o=0.79$, $s=2$,
$M_2=-1.71$, $\lambda_2=0$, $A_2'=0.7$

Fig. 4. 17. Stationary breakdown of double helix type in actual swirling flow field [by Eq. (3. 4)].

mode, and it represents the stationary breakdown of the double helix type (values of parameters are given under the figure). As seen from the comparison with Fig. 4.6(b) for the rigidly rotational flow with uniform axial velocity, both cases agree quite well with each other as to the essential character of flow pattern. This fact suggests the propriety of the foregoing discussions on the form of vortex breakdown, although they are founded on the assumption that the primary flow is rigidly rotational with uniform axial velocity.

4. 5. *Relation Between Axial Position of Various Types of Breakdown and Reynolds Number*

The relation between the axial positions where breakdowns appear and Reynolds number is discussed briefly. The experiment is carried out in the following manner, namely the flow rate is gradually changed for various values of vane angle ϕ. An example of obtained results is shown in Fig. 4.18. In the figure, the abscissa is the axial position Z of breakdown and the ordinate is Reynolds number.

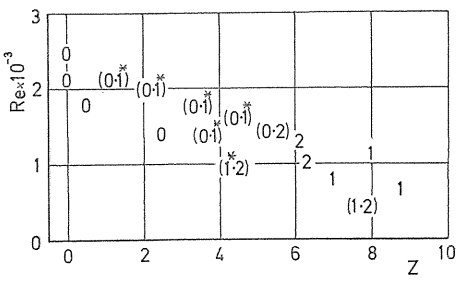

Fig. 4. 18. Axial position of various types of breakdown versus Reynolds number ($Z=0$ means upstream end of circular pipe).

The numbers 0, 1 and 2 written in the figure designate the elementary types of breakdown for $s=0$, 1 and 2, respectively. And the notation (0, 1), for example, denotes the breakdown which is explained as the coexistence of the disturbances of $s=0$ and 1 modes. The superscript $*$ indicates that the breakdown is unsteady. In classifying the types of breakdowns, the flow pattern which is shown in Fig. 4.4 (a), is regarded as type 0, and the kink type shown in Fig. 4.7 (a) is regarded as type (0, 1)*. Under the condition of constant vane angle, the form of breakdown varies with increasing Reynolds number in the following order, namely the steady spiral type, steady double helix type, unsteady spiral type (kink type) and axisymmetric type (bubble type). And the axial position of the breakdown shifts upstream in the same order. From the results of experiments for various vane angles, it is found that the order of the occurrence of breakdown is almost same for all cases. However, the Reynolds number for occurrence decreases with increasing the vane angle, and the axial position moves slightly upstream. These experimental results suggest that the occurrence of breakdown depends remarkably on the local state of the flow field. Finally, it should be added that, in the calculation of streaklines shown above, the finite values are taken for the amplitude of wave disturbances disregarding the postulation of an infinitesimal disturbance in the theoretical model. This is based on the conjecture that the infinitesimal disturbance hardly changes the shape in the growing process.

4. 6. Conclusions

In this chapter, propriety of the conception that the pattern of vortex breakdown depend on the mode of corresponding wave disturbance is confirmed by experiments. However, this study does not present the explanation of the developing mechanism and the precise expressions of the breakdown flow field. It is inferred that the former relates to the stability problem of the disturbance and the latter to a more accurate treatment of the nonlinear fundamental equations (the Euler or Navier-Stokes equations). These remain to be studied.

5. Nomenclature

a: radius of cylindrical vessel or circular pipe
D: diameter of circular pipe
l: length of cylindrical vessel
L: dimensionless value of l, $=l/a$
ρ: density
ν: kinematic viscosity
ϕ: angle of guide vane

r, θ, z : cylindrical coordinates
θ' : azimuthal angle in rotating cylindrical polar coordinate system
R : dimensionless value of r, $=r/a$
Z : dimensionless value of z, $=z/a$
u, v, w : velocity components in r, θ, z direction
$\bar{u}$, $\bar{v}$, $\bar{w}$: velocity components in r, θ, z direction of primary flow
$\tilde{u}$, $\tilde{v}$, $\tilde{w}$: velocity components in r, θ, z direction of disturbance
U_0 : mean velocity of primary flow in z direction
W_0 : velocity component in z direction of swirling flow with uniform axial velocity distribution
$\mathbf{U}$: dimensionless value of u, $=u/(a\Omega)$
$\mathbf{V}$: dimensionless value of v, $=v/(a\Omega)$
$\mathbf{W}$: dimensionless value of w, $=w/(a\Omega)$
$U(r)$, $V(r)$, $W(r)$: eigenfunctions of $\tilde{u}$, $\tilde{v}$ and $\tilde{w}$
p : static pressure
$\bar{p}$: static pressure of primary flow
$\bar{p}_0$: value of p on pipe axis
$\tilde{p}$: static pressure of disturbance
$P(r)$: eigenfunction of p
Ω : angular velocity of rotating flow with or without axial velocity component
t : time
T : dimensionless value of t, $=\Omega t$
τ : rotational period of streakline, $=2\pi s/|N|$
m : wave number of disturbance in z direction
s : wave number of disturbance in θ direction
n : angular frequency of disturbance
n' : angular frequency of disturbance viewed from rotating cylindrical polar coordinate system
σ : root of following equation;

$$J_{s-1}(\sigma a)/J_s(\sigma a)=(s/\sigma a)\{1\pm\sqrt{1+(\sigma/m)^2}\}$$

σ' : dimensionless value of σ, $=a\sigma$
λ : eigenvalue of disturbance
k : integer parameter for axial mode of elastoid-inertia oscillation, $=ml/\pi=1, 2, 3, \ldots$
g : integer parameter for radial mode of disturbance or of elastoid-inertia oscillation, $=1, 2, 3, \ldots$
n_e : experimental value of natural angular frequency of elastoid-inertia oscillation
n_f' : angular frequency of excitation
n_{fr}' : value of n_f' in resonant state
M : dimensionless value of m, $=am$
N : dimensionless value of n, $=n/\Omega$
N' : dimensionless value of n', $=n'/\Omega$
c : amplitude of elastoid-inertia oscillation
C : dimensionless value of c, $=c/(a\Omega)$
A : amplitude of disturbance
A' : dimensionless value of A, $=A/(a\Omega)$

R_o: Rossby number, $=W_0/(a\Omega)$
R_e: Reynolds number, $=DU_0/\nu$

Acknowledgement

To Mr. Takafuni Nakahama, Mr. Toshihide Niimi. Mr. Tetsuo Nakamura and Fujio Hori, we are very grateful for offering valuable suggestions for improvement of this research.

Mr. Hideo Matsuura has made for us many ingeneous instruments for our experiments.

Acknowledgement is made to the Nagoya University Computation Center for providing convenience for computation in this research.

References

1) Kito, F. and Uchimaru, S., "On the Vibrations of Draft Tube of Water Turbine", J. Faculty Eng. Tokyo Univ., Vol. 18, No. 8, Feb. 1930, p. 212.
2) Suzuki, M., "Theoretical and Experimental Studies on the Vortex-tube", Sci. Pap. Inst. Phys. Chem. Res., Vol. 54, 1960. p. 43.
3) Lord Kelvin, "Vibrations of a Columnar Vortex", Philos. Mag., Vol. 10, 1880, p. 155.
4) Bjerknes, V. and Solberg, H., "Physikalische Hydrodynamik", 1933, p. 421, Springer.
5) Greenspan, H. P., "The Theory of Rotating Fluids", 1969, Cambridge Univ. Press.
6) Long, R. R., "Steady Motion around a Symmetrical Obstacle Moving along the Axis of a Rotating Liquid", J. Meteorol., Vol. 10, 1953, p. 197.
7) Oser, H., "Experimentelle Untersuchung über Harmonische Schwingungen in Rotierenden Flüssigkeiten", Z. Angew. Math. Mech., Bd. 38, 1958, S. 386.
8) Fultz, D. "A Note on Overstability and the Elastoid-Inertia Oscillations of Kelvin, Solberg, and Bjerknes", J. Meteorol., Vol. 16, 1959, p. 199.
9) Peckham, D. H. and Atkinson, S. A., "Preliminary Results of Low Speed Wind Tunnel Tests on a Gothic Wing of Aspect Ratio 1.0", Aeronaut. Res. Counc., C. P. 508, 1957, p. 16.
10) Lambourne, N. C. and Bryer, D. W., "The Bursting of Leading-Edge Vortices, Some Observations and Discussion of the Phenomenon", Aeronaut. Res. Counc., No. 3282, 1961, p. 32.
11) Hümmel, D., "Untersuchungen über das Aufplatzen der Wirbel an schlanken Deltaflugeln", Z. Flugwiss., Bd. 13, 1965, S. 158.
12) Benjamin, T. B., "Some development in the theory of vortex breakdown", J. Fluid Mech., Vol. 28, part 2, 1967, p. 65.
13) Ludwieg, H., Erklärung des Wirbelaufplatzens mit Hilfe der Stabilitätstheorie für Strömungen mit schraubenlinienförmigen Stromlinien", Z. Flugwiss., Bd., 13, 1965, S. 437.
14) Hall, M. G., "The Structure of Concentrated Vortex Cores", Prog. Aeronaut. Sci., Vol. 7, 1966, p. 53.
15) Bossel, H. H., "Vortex Computation by the Method of Weighted Residuals Using Exponentials", AIAA J., Vol. 9, No. 10, 1971, p. 2027.
16) Leibovich, S., "Weakly non-linear waves in rotating fluids", J. Fluid Mech., Vol. 42, part 4, p. 803.
17) Randall, J. D. and Leibovich, S., "The critical state: a trapped wave model of vortex breakdown", J. Fluid Mech., Vol. 58. part 3, 1973, p. 495.

18) Grabowski, W. J. and Berger, S. A., "Solutions of the Navier-Stokes equations for vortex breakdown", J. Fluid Mech. Vol. 75, part 3, 1976, p. 525.
19) Sarpkaya, T., "On stationary and travelling vortex breakdowns" J. Fluid Mech., Vol. 45, part 3, 1971, p. 545.
20) Faler, J., and Leibovich, S., "Disrupted states of vortex flow and vortex breakdown", Phys. Fluids, Vol. 20, No. 9, 1977, p. 1385.
21) Nakamura, Y., et. al., "Experiments on vortex breakdown of the swirling pipe flow by the use of laser-Doppler velocimeter", 4th Symp. Flow Visualization ISAS, 1976, p. 41.
22) Ikeda, T., et. al., "Velocity Profile Measurements of a Swirling Flow associated with Vortex Breakdown by Oil Tracer Injection Method", 3rd Symp. Flow Visualization ISAS, 1975, p. 75.
23) Suematsu, Y. and Ito, T., "Vortex Breakdown Phenomena in a Circular Pipe (1st Report, Modes of Stationary Breakdown)", Bull. JSME, Vol. 24, No. 193, 1981, p. 1137.
24) Suematsu, Y., Ito, T., Niimi, T. and Nakamura, T., "Vortex Breakdown Phenomena in a Circular Pipe (2nd Report, Flow Modes of Unsteady Type Breakdowns)", Bull. JSME, Vol. 25, No. 199, 1982, p. 38.
25) Suematsu, Y., Ito, T., Hayase, T. and Hori, F., "Vortex Breakdown in a Circular Pipe (3rd Report, A Comparison Between Experimental and Theoretical Flow Patterns)", Trans. JSME, Vol. 47, No. 421, 1981, p. 1736.
26) Ito, T., Suematsu, Y., Hayase, T. and Nakahama, T., "Experiments on the Elastoid-inertia Oscillations of Rigidly Rotating Fluid in a Cylindrical Vessel", Bull. JSME, Vol. 27, No. 225, 1984, p. 458.